

1 **The impacts of fireworks burning at Chinese Spring Festival on air quality: insights of**
2 **tracers, source evolution and aging processes**

3 Shaofei Kong ^{1,2}, Li Li ², Xuxu Li ², Yan Yin ^{1,2*}, Kui Chen ^{1,2}, Dantong Liu ⁴, Liang Yuan ²,
4 Yingjie Zhang ², Yunpeng Shan ², Yaqin Ji ^{3*}

5 *1. Collaborative Innovation Center on Forecast and Evaluation of Meteorological*

6 *Disasters, Nanjing University of Information Science and Technology, Nanjing, 210044, China*

7 *2. Key Laboratory for Aerosol-Cloud-Precipitation of China Meteorological Administration, School of*
8 *Atmospheric Physics, Nanjing University of Information Science & Technology, Nanjing 210044, China*

9 *3. Colloge of Environemental Science and Engineering, Nankai University, Tianjin, 100086, China*

10 *4. School of Earth, Atmospheric and Environmental Science, University of Manchester, Manchester, UK*

11 **Abstract:**

12 To understand the impact of fireworks burning (FW) particles on air quality and human
13 health during winter haze period, thirty-nine elements, ten water-soluble ions and eight fractions
14 of carbonaceous species in atmospheric PM_{2.5} at Nanjing were investigated during 2014 Chinese
15 Spring Festival (SF). Serious regional haze pollution persisted throughout the entire sampling
16 period, with PM_{2.5} averaging at 113 ± 69 μg m⁻³ and visibility at 4.8 ± 3.2 km. The holiday effect led
17 to almost all the chemical species decreasing during the SF, except for Al, K, Ba and Sr which
18 were related to FW. The source contributions of coal combustion, vehicle emission and road dust
19 decreased dramatically, whereas FW contributed to about half of the PM_{2.5} during SF period. The
20 intensive emission of FW particles at New Year's Eve accounted for 60.1% of the PM_{2.5}.
21 **Fireworks** also obviously modified the chemical compositions of PM_{2.5}, with 39.3% contributed
22 by increased organic matter, followed by steadily increased loadings of secondary inorganic ions.
23 The aging processes of the FW particles lasted for about four days reflected by the variations of
24 Ba, Sr, NH₄⁺, NO₃⁻, SO₄²⁻ and K⁺, characterized by heterogeneous reactions of SO₂ and NO_x on
25 crustal materials directly from FW, the replacement of Cl⁻ by NO₃⁻ and SO₄²⁻, coating of NO₃⁻ and
26 SO₄²⁻ on soot, formation of secondary organic aerosols and metal-catalyzed formation of NO₃⁻ and
27 SO₄²⁻ at higher relative humidity. During aging, the main contributors to the extinction coefficient
28 shifted from elemental carbon and organic matter to ammonium sulfate. **The particles raised**
29 **higher cancer risk of 1.62 × 10⁻⁶ by heavy metals (especially for Cd and As).** This study provided
30 detailed composition data and first comprehensive analysis of the aging processes of FW particles

31 **during** serious haze pollution period and their potential impact on human health.

32 **Keywords:** PM_{2.5}; chemical compositions; haze; fireworks burning particles; aging; health risk

33

34 * *Correspondence to:* Y. Yin (yinyan@nuist.edu.cn); Y.Q. Ji (jiyaqin@nankai.edu.cn); S.F. Kong
35 (kongshaofei@126.com)

36 Address: Nanjing University of Information Science and Technology, Ningliu Road 219, Nanjing,
37 China; Tel/Fax: +86-25-58731207

38

39 **Abbreviations glossary:**

40 FW-Fireworks burning

41 CNY-Chinese New Year day

42 SF-Spring Festival

43 LF-Lantern Festival

44 OC-Organic carbon

45 EC-Elemental carbon

46 BC-Black carbon

47 OM-Organic matter

48 RH-Relative humidity

49 ICP-MS-Inductively coupled plasma-mass spectroscopy

50 ICP-OES-Inductively coupled plasma-optical emission spectrometer

51 OPC-Optically detected pyrolyzed carbon

52 PCA-Principal component analysis

53 LADD-Lifetime average daily dose

54 InhR-Inhalation rate

55 EF-Exposure frequency

56 ED-Exposure duration

57 BW-Average body weight

58 AT-Averaging time

59 HQ-Hazard Quotient

60 RfD-Reference dose

61 HI-Hazard Index

62 MIN-Mineral matter

63 TE-Trace elements

64 SS-Sea salt

65 SIA-Secondary inorganic aerosol

66 UM-Unidentified matter

67 R²-Correlation coefficient

68 WRF-Weather Research and Forecast model

69 Pre-CNY-The day before CNY

70 Pre-LF-The day before LF

71 Pre-SF-The period before Spring Festival
72 After-SF-The period after Spring Festival
73 PM_{cal} -Mass calculated by adding individual components
74 PM_{meas} -Gravimetrically measured particulate mass
75 V_{cal} -Visibility calculated by adding individual components
76 V_{meas} -Measured visibility
77 b_{ext} -Extinction coefficient

78

79 **1 Introduction**

80 Atmospheric pollutants emitted from fireworks burning (FW) at festivals or special
81 celebration events around the world have recently received wide attention, such as Guy Fawkes'
82 night at UK (Allan et al., 2010; Godri et al., 2010), Pyronale® 2009 and Pyromusikale®
83 (Dutschke et al., 2011), Montréal International Fireworks competition (Joly et al., 2010), New
84 Year's celebrations (Williams et al., 2005; Drewnick et al., 2006; Zhang et al., 2010; Do et al.,
85 2012; Feng et al., 2012; Jiang et al., 2014; Jing et al., 2014; Tian et al., 2014; Ye et al., 2014),
86 Diwali (Godri et al., 2010), Las Fallas in Valencia (Moreno et al., 2007), new Millennium in
87 Germany (Wehner et al., 2000), 2006 FIFA World Cup (Vecchi et al., 2008) and Lantern Festival
88 (Do et al., 2012; Tsai et al., 2012). Besides the direct possible dangers like the exposure to sound
89 pressures (Dutschke et al., 2011) or firework-related injuries (Do et al., 2012), their burning results
90 in massive quantities of pollutants, leading to degradation of air quality (Wang et al., 2007; Sarkar
91 et al., 2010; Dutschke et al., 2011; Do et al., 2012; Feng et al., 2012; Tsai et al., 2012; Jiang et al.,
92 2014; Jing et al., 2014; Tian et al., 2014; Yang et al., 2014) and raising serious human health
93 concerns (Godri et al., 2010; Do et al., 2012). Evidence suggests that inhalation of fumes
94 containing high levels of specific elements such as chlorine can cause mucosal irritation and acute
95 respiratory distress syndrome (Joly et al., 2010). A toxicity study reported that the samples
96 collected in the post-FW period were more toxic than those in the pre-FW period according to the
97 viabilities of BEAS-2B cells after 24-h incubation with the particle extracts (Do et al., 2012). A
98 positive significant relationship was also found between particulate matter oxidative burden and
99 individual trace metals associated with FW (Godri et al., 2010).

100 China is the largest firework producing country in the world (Tian et al., 2014). For the
101 Chinese New Year day (CNY, in the Spring Festival (SF) on Jan. or Feb. of lunar Chinese
102 calendar, high-profile FW events occurred at the midnight of the CNY's Eve in national scale,

103 from small villages to megacities. It should be noted that FW events always occurred in an already
104 highly polluted urban air in China ([Supplementary file S1](#)). In winter, increased coal consumption
105 for heating ([Li and Zhang, 2014](#)) and stable atmospheric conditions always raise serious haze
106 pollution in central and eastern China. On January 2013, the whole central and eastern China was
107 shrouded in a long-lasting severe haze episode ([Wang et al., 2014](#)). According to the Chinese
108 Ministry of Environmental Protection, on Jan. 31, 2014, about 80% of 161 cities held average
109 PM_{2.5} concentrations higher than 150 µg m⁻³ ([Ye et al., 2014](#)). The addition of pollutants from FW
110 deteriorates ambient air quality during the SF and its impact can vary significantly with FW
111 duration and meteorological conditions ([Vecchi et al., 2008](#); [Yu et al., 2013](#)).

112 Previous studies have extensively characterized the physicochemical signatures of FW
113 emissions, such as gaseous pollutants ([Wehner et al., 2000](#); [Attri et al., 2001](#); [Williams et al., 2005](#);
114 [Drewnick et al., 2006](#); [Wang et al., 2007](#); [Vecchi et al., 2008](#); [Tan et al., 2009](#); [Godri et al., 2010](#)),
115 particle size distribution and number concentration ([Wehner et al., 2000](#); [Drewnick et al., 2006](#);
116 [Vecchi et al., 2008](#); [Zhang et al., 2010](#); [Dutschke et al., 2011](#); [Yang et al., 2014](#)), chemical
117 components including trace elements ([Wang et al., 2007](#); [Moreno et al., 2007](#); [Vecchi et al., 2008](#);
118 [Estrellan and Iino, 2010](#); [Godri et al., 2010](#); [Joly et al., 2010](#); [Do et al., 2012](#); [Tsai et al., 2012](#);
119 [Tian et al., 2014](#); [Yang et al., 2014](#)), organic carbon (OC) and elemental carbon (EC) ([Estrellan
120 and Iino, 2010](#); [Feng et al., 2012](#); [Tsai et al., 2012](#); [Tian et al., 2014](#); [Yang et al., 2014](#)) and
121 water-soluble ions ([Wang et al., 2007](#); [Vecchi et al., 2008](#); [Shen et al., 2009](#); [Estrellan and Iino,
122 2010](#); [Tsai et al., 2012](#); [Wang et al., 2013](#); [Jiang et al., 2014](#); [Tian et al., 2014](#); [Yang et al., 2014](#)).
123 Recently, single particle's chemical compositions ([Drewnick et al., 2006](#); [Allan et al., 2010](#); [Jiang
124 et al., 2014](#)), morphology and mixing properties ([Li et al., 2013](#)) and optical properties ([Yu et al.,
125 2013](#)) of FW particles had been reported. **However, there are now still two issues needed to be
126 explicitly addressed.**

127 Firstly, no studies reported the chemical compositions (crustal elements, trace elements,
128 water-soluble ions, OC and EC) of FW particles completely, considering the complex manufacture
129 materials of FW ([Supplementary file S2](#)). Although [Estrellan and Iino \(2010\)](#), [Feng et al. \(2012\)](#),
130 [Yang et al. \(2014\)](#) and [Tian et al. \(2014\)](#) reported the ions, elements and carbonaceous species
131 synchronously, some important species were missed, such as Na, Mg, K, Ti, NH₄⁺ and Cl⁻ in [Tian
132 et al. \(2014\)](#), OC in [Estrellan and Iino \(2010\)](#), Si and some heavy elements in [Feng et al. \(2012\)](#)

133 and crustal elements in [Yang et al. \(2014\)](#). These species are all highly elevated during FW events.
134 Crustal elements including Na, Mg, Al, Si, K, Ca, Ti, Fe and Mn were always missing or not
135 sufficiently studied in FW particles. However, except for inorganic and organic chemicals such as
136 charcoal, potassium nitrate, potassium chlorate, potassium perchlorate, sulfur, manganese, sodium
137 oxalate, aluminum, iron powder, strontium nitrate, and barium nitrate ([Shen et al., 2009](#); [Jing et al.,](#)
138 [2014](#)), clay is also used to seal the top and bottom of fireworks as shown in [Supplementary file S3](#).
139 90% of the total mineral aerosol was from the emission of FW on the lantern night in Beijing
140 ([Wang et al., 2007](#)). The incomplete compositions of FW particles may bias the identification of
141 particle sources during FW period and limit our understanding of its aging processes. For example,
142 crustal elements-Al, Si and Ca were thought to result from the resuspension of materials already
143 deposited on the ground (caused by pyrotechnic device explosions) and hereby the resuspended
144 dust was regarded as a contributor to atmospheric particles during SF ([Tian et al., 2014](#)). Without
145 detecting the crustal and trace elements, secondary particulate matter accounted for 63-82% of
146 $PM_{1.0}$ during FW periods in Beijing ([Jiang et al., 2014](#)).

147 Secondly, all the former studies unanimously **agreed that** FW contributed to elevated
148 concentrations of particles and associated chemical species, but no studies concerned the aging
149 processes of particles after emitted from intensive FW. The cocktail of primary pollutants released
150 may exhibit varied interactions among themselves, and if aided by favourable atmospheric
151 conditions, may lead to the formation of secondary pollutants ([Sarkar et al., 2010](#)). [Do et al. \(2012\)](#)
152 pointed that the sub-micron aerosol or accumulation-mode particles from FW can suspend in the
153 air for very long periods, from days to weeks, potentially causing pollution to large areas. Data in
154 literature verified the existence of aging processes of FW particles, though it has not been
155 discussed. For example, [Li et al. \(2013\)](#) indicated that emissions from FW changed the
156 transformation pathway from SO_2 to SO_4^{2-} and the FW particles can influence the air at downwind
157 site (50 km far away). And after about two days, the elevated $PM_{2.5}$ mass concentrations at CNY's
158 Eve decreased to the level of the day before CNY (pre-CNY). In Beijing, $PM_{2.5}$ mass
159 concentrations at CNY's Eve decreased to the level of pre-CNY in one day, while secondary ions
160 (SO_4^{2-} , NH_4^+ and NO_3^-) and organic matter (OM) increased first and then decreased to the level of
161 pre-CNY after three days ([Wang et al., 2007](#)). In Jinan, a "tailing" phenomena was found,
162 indicating that NH_4^+ and NO_3^- did not increase (peaking at 8:00 and 12:00, respectively)

163 immediately with the concentrations of particles (peaking at 00:00) after emitted at CNY's Eve
164 (Yang et al., 2014). In Shanghai, NH_4^+ and NO_3^- also increased in the first day after emitted at
165 CNY's Eve and then decreased to the level of pre-CNY in the third day and the decreasing rate of
166 $\text{PM}_{2.5}$ was faster than that for OC (Feng et al., 2012). Therefore, we still need to answer the
167 following questions: (1) are the decreasing trends of particles and associated chemical components
168 the same? (2) how long and how far can FW influence the air quality at certain meteorological
169 conditions? (3) during aging and transport, which type of chemical reactions will the FW particles
170 undergo and how will specific chemical ratios vary?

171 Due to rapid economic expansion and urbanization, the occurrence frequency of haze has
172 increased rapidly in recent 30 years at the Yangtze River Delta region (Wang et al., 2014). As one
173 of the central megacities of this region, Nanjing is suffering from serious air pollution and the
174 occurrence of hazy days increased from 1961 to 2005 (Kang et al., 2013). Thus, it provides a
175 unique site and opportunity to study the chemical composition evolution and source variation
176 during haze-clear days with the injection of intensive FW at SF. The main purposes of this study
177 are to: (1) characterize in detail the chemical compositions of atmospheric $\text{PM}_{2.5}$ before, during
178 and after intensive FW events; (2) identify how long and how much can the FW particles
179 influence $\text{PM}_{2.5}$ by tracer analysis and receptor models; (3) emphasize how can the FW particles
180 affect visibility and human cancer and non-cancer risks; (4) analyze the FW particle aging
181 processes by specific species and ratios. The data and analysis will improve the knowledge of
182 chemical compositions of FW particles, their evolution during serious haze pollution periods and
183 their influence on visibility and human health.

184 **2 Methodology**

185 **2.1 $\text{PM}_{2.5}$ collection**

186 From 24 Jan. to 21 Feb. 2014, a sampling campaign of $\text{PM}_{2.5}$ was conducted on the rooftop
187 (40 m high) of a building in Nanjing University of Information Science & Technology (Kang et al.,
188 2013; Wang et al., 2014). It is a suburban site, surrounded by residential communities at the west,
189 south, north and southeast directions. There is a steel factory 2 km to the east of the campus and a
190 chemical industry park about 10 km to the northeast. It faced one road with heavy traffic, about
191 200 m in the east. Location of the sampling site was shown in Fig.1 and Supplementary file S4.
192 During the sampling period, CNY on Jan. 30 and Lantern Festival (LF) on Feb.14 were included.

193 At CNY's and LF's Eve, numerous fireworks were consumed. The SF holiday was from Jan. 30 to
194 Feb.7. Each day, PM_{2.5} samples were collected at about 08:00 am for 24 h using two
195 medium-volume air samplers (TH-150C, Wuhan Tianhong Ltd., China) on quartz fiber filters
196 (baked at 800 °C for 2 h) and polypropylene fiber filters (baked at 80 °C for 0.5 h) at a flow rate of
197 100 L min⁻¹. The hourly online PM_{2.5} mass concentrations for the nine monitoring sites set by
198 Jiangsu Environmental Monitoring Center were collected from the public platform
199 (<http://218.94.78.75/jsair/>) (their locations can be found in [Supplementary file S4](#)). Twenty-four
200 pairs of filter samples were obtained ([Supplementary file S5](#)). By using a microbalance (Ohaus
201 Discovery DV214CD) with balance sensitivity as ±0.010 mg, filters were weighed before and
202 after sampling under controlled environment with temperature and relative humidity (RH) of
203 22 °C and 35%. Then they were stored at -20 °C until chemical analysis. The quartz fiber filters
204 were for analyzing water-soluble inorganic ions, OC and EC. Polypropylene fiber filters were for
205 elemental analysis.

206

207 (Fig.1)

208

209 2.2 Chemical analysis

210 Inductively coupled plasma-mass spectroscopy (ICP-MS) (Agilent 7500a, Agilent Co. USA)
211 was used for analyzing Li, Be, Na, Mg, Al, P, K, Ca, Sb, Sc, Ti, V, Cr, Mn, Co, Ni, Cu, Zn, As, Rb,
212 Y, Mo, Cd, Sn, Cs, La, Ce, Sm, W, Tl, Pb, Bi, Th and U. Nine elements including Si, Al, Ca, Mg,
213 Fe, Ti, Ba, Sr and Zr were analyzed by inductively coupled plasma-optical emission spectrometer
214 (ICP-OES). Al, Ca, Mg and Ti were analyzed by both ICP-MS and ICP-OES, and results from the
215 latter were used as the analysis accuracy for the four elements by ICP-OES was better than that by
216 ICP-MS ([Kong et al., 2014a](#)). Ten ions including NH₄⁺, Na⁺, Mg²⁺, K⁺, Ca²⁺, F⁻, Cl⁻, NO₂⁻, NO₃⁻
217 and SO₄²⁻ were analyzed by a professional Ion Chromatograph (Wan Tong 850, Switzerland). DRI
218 Model 2001 (Thermal/Optical Carbon Analyzer) with the IMPROVE thermal/optical reflectance
219 protocol was used for OC and EC analysis ([Han et al., 2008](#); [Han et al., 2010](#); [Huang et al., 2012](#);
220 [Li et al., 2012](#); [Wang et al., 2013](#); [Kong et al., 2014a](#)). A 0.188 cm² punch area from the quartz
221 filter was heated to produce four OC fractions: OC1, OC2, OC3 and OC4 at temperatures of 120,
222 250, 450 and 550°C in a non-oxidizing He atmosphere, three EC fractions: EC1, EC2 and EC3 at

223 550, 700 and 800°C in an oxidizing atmosphere of 2% O₂/98% He and optically detected
224 pyrolyzed carbon (OPC). OC is defined as OC1+OC2+OC3+OC4+OPC and EC is calculated by
225 EC1+EC2+EC3-OPC. Char-EC is defined as EC1 minus OPC, and soot-EC is the sum of EC2 and
226 EC3 (Han et al., 2008; Han et al., 2010). The pre-treatment and chemical analysis procedures and
227 quality assurance and control are described detailedly in our previous works (Li et al., 2012; Kong
228 et al., 2014a; 2014b; Li et al., 2014).

229 **2.3 Meteorological parameters**

230 The meteorological parameters including relative humidity (RH), visibility, wind speed, wind
231 direction and temperature were recorded by the meteorological observatory of our university
232 (<http://qxt.nuist.edu.cn/>). The rainfall information was obtained from
233 <http://www.wunderground.com/>. According to China Meteorological Administration, fog is defined
234 as visibility <10 km and RH>90% and haze is defined as visibility <10 km and RH<80%. For
235 visibility <10 km and 80%<RH<90%, it is fog-haze mixing day. Fig.2 shows that the visibilities
236 are generally below 10 km (averaged as 4.8±3.2 km), indicating fog, haze or fog-haze mixing
237 events frequently occurred. On Feb.4, a strong cold front passed through, leading to high visibility
238 (14.7 km), low temperature (2.4°C) and high wind speed (3.5 m s⁻¹). The wind speed remained
239 mostly below 3 m s⁻¹ (averaged as 2.2±0.7 m s⁻¹), suggesting stagnant weather conditions.

240

241 (Fig.2)

242

243 **2.4 Data processing**

244 **2.4.1 Back trajectory calculation**

245 Three-day air mass back trajectories are calculated using NOAA Air Resource Lab HYSPLIT
246 4.8 model, driven by the GDAS meteorological dataset (1°×1°) (Kong et al., 2014b). A 72 h back
247 trajectory is adopted with the starting height of 500 m above ground level (Huang et al., 2012).
248 Cluster analysis is adopted which results in sub-sets of trajectories with backward trajectories
249 computed every six hours (00:00, 06:00, 12:00 and 18:00) each day. The clustering process is
250 described in detail in Hysplit User's Guide-Version 4. The mixing layer height is calculated every
251 three hours each day by the NOAA's READY Archived Meteorology online calculating program
252 (<http://ready.arl.noaa.gov/READYamet.php>). This program produces a time-series of calculated

253 boundary layer depth using the chosen meteorological data. As shown in Fig.3, 43% (cluster 3, 4
 254 and 5) of the air masses originated from the Mongolia and crossed Chinese coastal seas; 31%
 255 (cluster 1) was from the north China and transported across Shandong peninsula; 26% (cluster 2)
 256 was from central China. Cluster 1 and cluster 2 transported for short distances, which may easily
 257 raise regional air pollution, as the Shandong peninsula and central and eastern China hold
 258 intensive anthropologic sources for air pollutants.

259

260 (Fig.3)

261

262 2.4.2 Principal component analysis

263 Principal component analysis (PCA) is used to identify the sources for particles at periods
 264 before (Jan. 24-29), during (Jan. 30-Feb. 6), after SF holiday (Feb. 12-Feb. 21) and the whole
 265 period. It can analyze multivariate data sets structure and identify a smaller number of independent
 266 factors to explain the data variance. Factor loadings are related to the source emission
 267 compositions. A varimax normalized rotation is adopted by SPSS 13.0 software in this study
 268 (Kong et al., 2010).

269 2.4.3 Health risk assessment of heavy metals

270 After emitted, the heavy metals in FW particles can raise risks to human health. To raise the
 271 attention of public on the health threat of FW particles, the average amount of heavy metal
 272 exposure by inhalation (D_{inh}) per an individual's body weight over a given time span for adult and
 273 children was calculated by following equation (Kong et al., 2012; Yang et al., 2014):

$$274 \quad D_{inh} (mg \cdot kg^{-1} \cdot day^{-1}) = \frac{C \times InhR \times EF \times ED}{BW \times AT} \quad (1)$$

275 The lifetime average daily dose (LADD) of Co, Ni, As and Cd exposure through inhalation
 276 was used for assessing cancer risk as following:

$$277 \quad LADD = \frac{C \times EF}{AT} \times \left(\frac{InhR_{child} \times ED_{child}}{BW_{child}} + \frac{InhR_{adult} \times ED_{adult}}{BW_{adult}} \right) \quad (2)$$

278

279 where C is exposure-point concentration. Its upper limit of the 95% confidence interval for
 280 the mean is calculated as:

281
$$C_{95\%UCL} = \exp\left(\bar{X} + 0.5s^2 + \frac{s \times H}{\sqrt{n-1}}\right) \quad (3)$$

282 where \bar{X} is the arithmetic mean of the log-transformed data, s is the standard deviation of the
 283 log-transformed data, H is the H-statistic and n is the number of samples. InhR: inhalation rate, 7.6
 284 and 20 m³ day⁻¹ for children and adult; EF: exposure frequency, 4 day year⁻¹ in this study
 285 (according to the discussion in Section 3.4.2); ED: exposure duration, 6 and 24 years for children
 286 and adult; BW: average body weight; 15 and 70 kg for children and adult; AT: the averaging time,
 287 for non-carcinogens, AT (days)=ED×365; for carcinogens, AT (days)=70×365=25, 550.

288 After the D_{inh} is calculated, a Hazard Quotient (HQ) for non-cancer toxic risk can be obtained
 289 by (Kong et al., 2012):

290
$$HQ = D/RfD \quad (4)$$

291 Considering the sensitive group, the reference dose (RfD) (mg/kg/day) is estimated as the
 292 maximum permissible risk on human by daily exposure. The threshold values of RfD indicate
 293 whether there is adverse health effect during a life time. Then Hazard Index (HI) can be obtained
 294 by suming up the individual HQ to estimate the total risks of all elements considered:

295
$$HI = \sum HQ_i \quad (5)$$

296 where i denotes different heavy metals. RfD values are 7×10^{-3} , 2.86×10^{-5} , 1.43×10^{-5} ,
 297 4.0×10^{-2} , 3.0×10^{-1} and 3.5×10^{-3} for the cancer risk estimation of V, Cr, Mn, Cu, Zn and Pb. For
 298 non-cancer risk estimation of Co, Ni, As and Cd, the RfD values are 5.71×10^{-6} , 2.00×10^{-2} ,
 299 3.00×10^{-4} and 1.00×10^{-3} , respectively (Kong et al., 2012). If $HI \leq 1$, there is no adverse health
 300 effects; if $HI > 1$, likely adverse health effects exist. For carcinogens, the LADD is multiplied by
 301 the corresponding RfD value (they are 9.8×10^0 , 8.4×10^{-1} , 1.51×10^1 and 6.3×10^0 for Co, Ni, As
 302 and Cd, respectively) (Kong et al., 2012). For cancer risk, the value of 10^{-6} is an internationally
 303 accepted precautionary or threshold value above which the risk is unacceptable (Granero and
 304 Domingo, 2002; Baptistaa and Miguel, 2005).

305 2.4.4 Mass closure of PM_{2.5}

306 To better understand the chemical compositions before, during and after SF, the chemical
 307 mass closure analysis was conducted. The chemical components are divided into six classes as
 308 follows: mineral matter (MIN), trace elements (TE), OM, EC, sea salt (SS), secondary inorganic

309 aerosol (SIA) and unidentified matter (UM). MIN is the sum of the common oxides of Al, Mg, Mn,
310 Si, Na, K, Ca, Ti and Fe as:

$$311 \text{ MIN}=2.14 \times \text{Si}+1.67 \times \text{Ti}+1.89 \times \text{Al}+1.59 \times \text{Mn}+1.67 \times \text{Mg}+1.95 \times \text{Ca}+1.35 \times \text{Na}+1.21 \times \text{K}+1.43 \times \text{Fe} \quad (6)$$

312 As the existence of CaO and CaCO₃, a factor of 1.95 for Ca is used (Terzi et al., 2010).

313 Except for the above elements in MIN, all other elements are summed up to act as TE. OM is
314 calculated by multiplying OC of a conversion factor, in accordance with the organic molecular
315 carbon weight per carbon weight. The factor 2.0 is applied here, which is also used for spring
316 festival period in Shanghai, another megacity at Yangtze River Delta region (Huang et al., 2012).
317 In Allan et al. (2010), during bonfires and fireworks burning period at the Guy Fawkes' night, the
318 OM/OC ratio ranged around 2.0 or higher than 2.0. The marine contribution is calculated based on
319 a standard sea water composition, assuming that soluble Na⁺ in aerosols only come from sea salt.

320 Then,

$$321 \text{ sea salt}=[\text{Na}^+]+[\text{ss-Cl}^-]+[\text{ss-Mg}^{2+}]+[\text{ss-K}^+]+[\text{ss-Ca}^{2+}]+[\text{ss-SO}_4^{2-}] \quad (7)$$

322 where ss-Cl⁻=1.8×[Na⁺], ss-Mg²⁺=0.12×[Na⁺], ss-K⁺=0.036×[Na⁺], ss-Ca²⁺=0.038×[Na⁺],
323 and ss-SO₄²⁻=0.252×[Na⁺] (Terzi et al., 2010). SIA is the sum of nss-SO₄²⁻, NO₃⁻ and NH₄⁺. The
324 concentrations of all these species in μg m⁻³ are adopted.

325 2.4.5 Visibility re-construction by chemical components

326 The mass scattering efficiency of spherical particles is a function of water and chemical
327 components including (NH₄)₂SO₄, sea salt, mineral materials and carbonaceous species (Kim et al.,
328 2001). To find which types of chemical components are the key for the visibility degradation during
329 sampling period and how can the injection of FW particles change the visibility, the IMPROVE
330 equation was used to calculate the light extinction coefficient (b_{ext}) (Kim et al., 2001; Yang et al.,
331 2007):

$$332 b_{\text{ext}}=3f(\text{RH})[\text{ammonium sulfate}]+3f(\text{RH})[\text{ammonium nitrate}]+4[\text{OM}]+1[\text{soil}]+10[\text{BC}] \quad (8)$$

333 The visibility can be calculated by V_s= 3.91/b_{ext} (Yang et al., 2007). We used [ammonium
334 sulfate]=0.944×[NH₄⁺]+1.02×[SO₄²⁻], [ammonium nitrate]=1.29×[NO₃⁻], [OM]=2.0×[OC],
335 [soil]=MIN and [BC]=[EC] (Yang et al., 2007; Tao et al., 2009). f(RH) is the RH growth function
336 indicating how scattering efficiencies increase for SO₄²⁻ and NO₃⁻ as they absorb liquid water and
337 detailed data can be found in Tao et al. (2009).

338 2.4.6 WRF-FLEXPART modeling

339 To see the transport distance and decreasing trend of the highest mass concentrations of
340 PM_{2.5} at CNY's Eve, Weather Research and Forecast model (WRF) version 3.4 was used to
341 provide meteorological inputs of FLEXPART, with the NCEP global reanalysis meteorological
342 dataset (1°×1°) as initial and boundary conditions. The time step is set as 180 s. The grid system is
343 divided into 28 layers in the vertical direction. Two domains are adopted, with the grid resolutions
344 of 30 and 10 km. The simulating time period is 02:00-11:00 of Jan.31, 2014. The output of 10 km
345 evolution wind farms is used as the input of FLEXPART. For forward simulating of FLEXPART
346 model, Nanjing (N31°14'-32°37', E118°22'-119°14', height as 50 m) is considered as a whole
347 source region. In this study, we only considered the dry and wet deposition of particles at CNY's
348 Eve. The average mass concentration of 572 μg m⁻³ is used as the initial particle concentration.

349 3 Results and discussion

350 3.1 Comparison of particles before, during and after Chinese Spring Festival

351 3.1.1 PM_{2.5} mass concentrations

352 The concentrations of PM_{2.5} (averaged as 113±69 μg m⁻³, min-max: 21-318 μg m⁻³) in this
353 study by filter sampling varied consistently with those for the nine online monitoring sites set by
354 local government at urban Nanjing (averaged as 112±70 μg m⁻³, min-max: 13-385 μg m⁻³)
355 (Fig.2b). They correlated well with correlation coefficient (R²) higher than 0.95 (P>0.01)
356 (Supplementary file S6), indicating that a regional air pollution occurred in Nanjing (visibility<10
357 km as Fig.2a shown) during study period. The PM_{2.5} concentrations all peaked on CNY (Jan. 30)
358 and LF (Feb.14) and the peaking values on CNY were 4-5 times of the secondary standard of
359 China National Ambient Air Quality (75 μg m⁻³, 24 h average). Results suggested that FW have
360 obvious impacts on fine particle pollution. At CNY's Eve, two massive FW events usually occur
361 at the evening (around 19:00-20:00 h for the family reunion dinner) and midnight (00:00-02:00 h
362 for celebrating the new year). PM_{2.5} showed the maximum concentrations for the two episodes as
363 426±236 (20:00 h) and 572±136 μg m⁻³ (02:00 h), respectively (Fig.4). After 02:00, obviously
364 decreasing trend was pronounced as exponential form (R²=0.99). The concentrations decreased to
365 195±16 μg m⁻³ at 13:00, which was similar to that of 178±16 μg m⁻³ at 17:00, Jan. 30 before
366 extensively FW activities (Fig.4). Note that on Jan. 30 and Jan. 31, the mixing layer heights were
367 only 257 and 227 m, the wind speeds were 1.7 and 2.1 m s⁻¹ and the RH were 88 and 80%, all

368 favoring the accumulation of pollutants and regional air pollution formation. It was verified by the
369 WRF-FLEXPART results which indicated that the particles with highest mass concentrations at
370 02:00 moved outside of Nanjing in the following nine hours. The center with peaked particle mass
371 concentrations transported about 285 km to the north of Naning (Supplementary file S7) and the
372 decreasing trend was in accordance with the real particle concentrations decreasing (Fig.5). The
373 injection of FW particles deteriorated the air quality, with visibilities decreasing to 1.4-6.2 km in
374 the following four days. Therefore, the PM_{2.5} pollution raised by FW can last for about four days
375 under unfavorable weather conditions (visibility was strongly related to PM_{2.5} mass in Jan
376 30-Feb.3, R²=0.82). On Feb.3 and Feb.5, PM_{2.5} was cleaned effectively by the rainfall
377 (precipitation as 0.3 and 9 mm), decreasing by 5.6-10.6 times for the ten sites.

378

379 (Fig.4)

380

381 (Fig.5)

382

383 3.1.2 Characterization of chemical species

384 Table 1 and Table 2 summarized the statistics of PM_{2.5}, water-soluble ions, OC and EC
385 before, during and after SF. The data of CNY and LF were listed separately for intensive FW
386 activities. The ratios of PM_{2.5} and chemical species on CNY and LF with those for the day before
387 them were also listed. For elements, K, Si, Al, Na, Ca and Fe were the most abundant species,
388 totally accounting for 85%-90% of all the elements at these five periods. Without considering the
389 data for CNY, elements Al, K, Ba and Sr at SF still elevated when compared with those for Pre-SF,
390 whereas all other elements decreased during SF. This was related to the weakened sources, like
391 construction activities, vehicle emission and industrial activities in the national holiday. For ions,
392 NO₃⁻ was most abundant, averaging as 5.9 (±3.7) μg/m³ for the days without intensive FW
393 activities, then followed by SO₄²⁻ and NH₄⁺, with average concentrations of 5.0 (±3.7) and 4.8
394 (±2.4) μg m⁻³, respectively. K⁺ and Cl⁻ also had relatively high concentrations of 0.9 (±1.0) and 0.8
395 (±0.5) μg m⁻³. It was similar to the results of Wang et al. (2014) that the secondary aerosols in
396 Nanjing were dominated by nitrate in winter haze periods. Na⁺, Ca²⁺, Mg²⁺, F⁻ and NO₂⁻
397 accounted for a minor fraction (totally of 4.2%). For carbonaceous species, OC3, OC4 and EC1

398 were most abundant, in combination accounting for 80% of the total carbon, indicating coal
399 combustion and gasoline exhaust were important sources for PM_{2.5} at Nanjing (Cao et al., 2005).
400 OPC and OC1 also showed a higher values which may be related to biomass burning (Cao et al.,
401 2005). NO₃⁻, OC and EC were highest for Pre-SF period, as the “spring travel rush” effect,
402 characterized by extremely high traffic flows (Huang et al., 2012). The PM_{2.5} concentrations
403 decreased for about 10 μg m⁻³ during SF, implying that the reduction of anthropogenic sources in
404 this national holiday (Feng et al., 2012). The particle concentration lower than that for pre-holiday
405 period was also found in Shanghai (Huang et al., 2012).

406 During CNY with intensive FW, concentrations of Ba and Sr exhibited the most significant
407 increase, by factors of 99.1 and 79.4 compared to the day before CNY (Pre-CNY). Ba and Sr also
408 showed the highest ratios for LF/Pre-LF (the day before LF), as 9.7 and 5.7, respectively. Then
409 followed by EC2, OC1, K, K⁺, Al, Bi, SO₄²⁻, OC2, EC1 and OC, going up to 4.1-37.7 times for
410 CNY/Pre-CNY, respectively. Other species increased by 1.2-3.8 times except for W (0.6), Na⁺
411 (0.7), NO₂⁻ (0.8) and OC4 (0.9). It implied that Na⁺ was not affected by the FW and can be used as
412 the tracer of sea salt. Most species also increased on LF when compared with Pre-LF, but the
413 increasing ratios were much lower than those on CNY. It can be explained as the FW activities on
414 LF (there are only organized FW activities by some organizations at cities) were less intensive
415 than those on CNY (FW activities are national spread, from city to small villages). Crustal
416 elements like Li, Be, Si, Na, Ca, Ti and Mn increased by about 1-2 times during FW, indicating
417 the use of clay in firework production. Ca²⁺ and EC1 decreased by factors of 0.8 and 0.9,
418 suggesting the increase of construction activities and vehicle emissions after SF. Meanwhile, Ba
419 and Sr tend to be tracers of firework (R²=0.99), consistent with former studies (Estrellan and Iino,
420 2010; Sarkar et al., 2010; Feng et al., 2012). As shown in the supplementary file S2 and literature
421 (Moreno et al., 2007; Vecchi et al., 2008; Joly et al., 2010; Sarkar et al., 2010; Richard et al., 2011;
422 Do et al., 2012; Tsai et al., 2012; Jing et al., 2014), the compounds of these elements are important
423 FW manufacturing materials. Barium compounds can be used as oxidiser (BaClO₃ and Ba(NO₃)₂).
424 Sr(NO₃)₂ can be used to give red color fireworks and potassium compounds are the most
425 important compositions of black powder (as KNO₃ or KClO₃). Al is used alone as a common
426 constituent for fuel, or to form sparks and glitter effects or as alloy magnalium (50:50 Mg:Al) for
427 sparks and crackling stars. Fireworks also contain charcoal (Joly et al., 2010; Sarkar et al., 2010;

428 Tsai et al., 2012) and organic materials are used as adhesive, such as polyvinyl alcohol,
429 polyoxyethylene, phenol formaldehyde resin and shell-lac. They are responsible for the elevated
430 concentrations of EC2 (Joly et al., 2010; Sarkar et al., 2010; Tsai et al., 2012) and OC1 during FW
431 periods.

432

433 (Table 1)

434

435 (Table 2)

436

437 3.2 Mass closure and re-construction of visibility

438 Fig. 6 illustrates the PM_{2.5} mass balance of MIN, TE, OM, EC, SS, SIA and UM. About 60%
439 of the chemical species in PM_{2.5} were detected. The unaccounted PM mass were explained by the
440 following four reasons: (1) non-C atoms in organic aerosols; (2) sampling and measurement
441 artifacts; (3) conversion factors used for OM and MIN calculating; (4) aerosol water content
442 (Tsyro, 2005; Terzi et al., 2010). Water constituted 20-35% of the annual mean PM₁₀ and PM_{2.5}
443 concentrations (Tsyro, 2005). On Feb. 6, the water content in PM_{2.5} was high to 72%, indicating
444 the influence of rainfall and high RH (90%). These also lead to the gravimetrically measured
445 particulate mass (PM_{meas}) higher than the mass calculated by adding individual components
446 (PM_{meas}), while tight correlations still existed between them ($PM_{meas}=1.52PM_{cal}+14.5$, $R^2=0.91$).
447 The slope was similar to those as 1.02-1.42 in Terzi et al. (2010).

448

449 (Fig.6)

450

451 The averaged chemical components of PM_{2.5} profiles exhibited OM (26%)>SIA (18%)>MIN
452 (9%)>EC (3.9%)>SS (1.7%)>TE (0.67%). The mass percentages of OM, TE and EC decreased in
453 SF (as 23%, 0.6% and 2.7%) when compared with those at Pre-SF (as 34%, 0.7% and 6.2%).
454 These changes reflected the holiday effect i.e. at the SF holiday, the new injection of FW particles
455 cannot offset the reduced particles from vehicle emission and/or to industrial sources, especially
456 for organic matter, trace elements and elemental carbon, which are important compositions of
457 vehicle exhausts and industrial activities. On CNY, obviously elevated OM was observed,

458 accounting for 39.3% of PM_{2.5}. While SIA was only 14.4%, with the peak values occurred on
459 Feb.3 (as 36%), suggesting that after intensive emission of FW pollutants on CNY's Eve,
460 secondary ions were gradually formed during aging processes through gas-particles transformation
461 of SO₂ and NO_x, etc. It should be emphasized that MIN and TE were both important components
462 of PM_{2.5}, totally accounting for 5.8%-18.5%. In a recent study by AMS for aerosols during
463 Chinese Spring Festival at Beijing, organics, nitrate, sulfate, ammonium, BC and chloride,
464 accounted for 43%, 22%, 14%, 13%, 5% and 3% of PM_{1.0} with no elements considered (Jiang et
465 al., 2014). The combination of filter sampling-offline chemical analysis and online real-time
466 monitoring of chemical species are desired for atmospheric aerosol studies.

467 Fig. 7a shows the calculated average values of extinction coefficient (b_{ext}). They varied
468 between 44 and 525 Mm⁻¹. The calculated visibility (V_{cal}) exhibited good correlations with the
469 measured one (V_{meas}) ($V_{\text{cal}}=0.96V_{\text{meas}}+1.4$, $R^2=0.45$, $P<0.001$). The discrepancy between the
470 measured and calculated values can be attributed to the influence of ambient water vapor (Huang
471 et al., 2012) which was a key component of aerosol particles in this study as discussed before. At
472 higher RH, the role of ambient water vapor on light extinction was more important (Huang et al.,
473 2012). The b_{ext} exhibited higher values on CNY and the following three days, in the range of
474 301-525 Mm⁻¹. (NH₄)₂SO₄ had the largest contribution to b_{ext} , accounting for 36.5±1.7%,
475 followed by NH₄NO₃ (25.8±8.2%), EC (21.8±9.0%), OM (10.8±4.2%) and soil (5.1±1.8%)
476 (Fig.7b). These results implied that sulfate was the largest contributor to visibility degradation
477 especially at SF period. Before SF, the contribution of EC can be as high as 34%-44% during
478 serious haze periods (Jan. 24-26, RH<51%). It highlights the importance of controlling vehicle
479 emissions in haze days. Sulfate and soot were also found as the main contributors to visibility
480 degradation in other studies (Tao et al., 2009). The results obtained here were different from those
481 in Shanghai that organic aerosol had the largest contribution to the aerosol extinction as 47 %,
482 then followed by ammonium sulfate (22%), ammonium nitrate (14 %) and EC (12 %) (Huang et
483 al., 2012). The FW on CNY obviously changed the contributions of chemical species to scattering
484 coefficient. On CNY, the influence of FW particles on visibility was mainly controlled by
485 (NH₄)₂SO₄ (36%), NH₄NO₃ (26%), EC (15%) and OM (15%). During FW particle aging
486 processes, the contribution of (NH₄)₂SO₄ increased from 36% (Jan.30) to 67% (Feb.3), while for
487 NH₄NO₃, its contribution increased first to 28% on Jan.31 and then decreased to 10% (Feb.3).

488 Similar trend was found for EC, it increased to 22% (Feb.1) and then decreased to 7.6% (Feb.3).
489 For OM, it exhibited decreasing trend, to the lowest value on Feb.2 (5.5%).

490

491 (Fig.7)

492

493 3.3 Source evolution

494 3.3.1 Contributions of fireworks burning to PM_{2.5} on CNY and LF

495 The PM_{2.5} concentrations peaked on CNY and LF in this study with intensive FW activities.
496 Assuming that the PM_{2.5} collected on CNY and LF was a simple combination of particles from
497 FW and other emission sources, the contribution and compositions of the particles from FW can
498 be estimated by subtracting the contribution of the non-firework sources (Feng et al., 2012). An
499 accumulation factor of 0.88 (mixing layer heights on Jan. 30 and Jan. 29 were 227 and 257 m,
500 respectively) and 0.51 (mixing layer heights on Feb. 14 and Feb. 13 were 353 and 696 m,
501 respectively) were used to eliminate the disperse impact caused by mixing height layer increasing
502 (Feng et al., 2012; Deka and Hoque, 2014). About 60.1% and 10.9% of the PM_{2.5} masses on CNY
503 and LF were estimated to be from FW. The contributions to almost all species of FW on CNY
504 were more obvious than those during LF (Fig.8). On CNY, OPC, EC3, Ba, Sr, Soot-EC, EC2 and
505 OC1 maintained the higher contributions from FW, larger than 80%, followed by K, K⁺, Al, Bi
506 and Char-EC, with the contributions higher than 70%. On LF, 45% of Ba and 41% of Sr were
507 from FW and the contributions to V, Bi, Fe, Be, K, K⁺, Al, NO₂⁻ and Sb were higher than 20%.

508

509 (Fig.8)

510

511 3.3.2 Source variations by tracers and PCA analysis

512 In order to further identify the sources of particles, PCA results are shown in Fig.9 and
513 supplementary file S8.

514

515 (Fig.9)

516

517 Five, five and eight factors were extracted for the dataset of Pre-SF, SF and After-SF period,

518 which explained 100%, 99.4% and 97.5% of the variance, suggesting almost all the sources have
519 been explained. Fireworks burning was the most important source for PM_{2.5}, contributing 24.0%
520 for the whole period. Coal combustion (including both local and regional transport) was also
521 important to PM_{2.5} at this site in winter (contributing 19.3%). It was verified by the time series of
522 tracers (As and Sb, highly correlated with R²=0.88) for coal combustion in Fig.10a. Extremely high
523 values can be found on Jan. 24, even higher than those for the intensive FW day. This can be
524 explained by two reasons: (1) on Jan. 24, it was a haze day with visibility and mixing layer height
525 as 8.2 km and 321 m, facilitating the accumulation of pollutants; (2) the air masses on Jan.24 were
526 classified as cluster 2 from central China where the Chang-Zhu-Tan region with intensive
527 non-ferrous metal metallurgy industries with huge coal consumption is located. On this day,
528 higher concentrations were also found for metals like Mg (228 ng m⁻³), Cr (17 ng m⁻³), Ca (782 ng
529 m⁻³), Mn (85 ng m⁻³), Fe (1014 ng m⁻³), Co (0.61 ng m⁻³), Ni (7.6 ng m⁻³), Cu (124 ng m⁻³), Mo
530 (4.4 ng m⁻³), Cd (8.8 ng m⁻³), Sn (16 ng m⁻³) and Pb (359 ng m⁻³). FW contributed about half of
531 the PM_{2.5} during SF period. For Pre-SF and after-SF periods, its contributions were 9% and 14%.
532 As shown in Fig.10b, the tracers of Ba and Sr exhibited much higher values at SF, and there were
533 also some small peaks before SF (Jan. 27) and after SF (Feb. 14). During the one-week holiday,
534 most industrial activities shut down in China with low energy consumption during this period
535 (Feng et al., 2012; Huang et al., 2012; Li et al., 2013). As holiday effect, when compared the
536 source contributions at SF to those at Pre-SF, the contributions of coal combustion decreased from
537 46% to only 16%, the contributions of vehicle emissions decreased from 17% to 14% and the
538 contributions of dust also decreased. For After-SF period, along with the gradually re-starting of
539 industrial/construction activities and the increasing of traffic flows, the source contributions of coal
540 combustion, heavy oil burning, industrial processes and road dust increased, to 37%, 4%, 3.4%
541 and 5%, respectively. OC and EC were selected as the tracers of vehicle emission and their
542 correlation was higher to 0.80 without the data on CNY and LF. Ca was selected as the tracer for
543 construction activities or road dust (the main road was covered by abundant dust from subway
544 construction). Na⁺ was used as the tracer of sea salt. Li, Be and Si were selected as the indicators
545 of soil (R² higher than 0.65 between them). The variations of mass concentrations of these tracers
546 before, during and after SF coincided with the contributions of corresponding sources.

547

(Fig.10)

548

549

550 3.4 Aging processes

551 3.4.1 The aging processes and mechanisms of fireworks burning particles

552 Previous studies indicated that the aerosol emission from FW activities is a short-term air
553 quality degradation event (Jing et al., 2014), but no studies concerned how long the duration time
554 is, and during the aging processes, what are the substantial hazard risk levels raised by elevated
555 heavy metals from intensive FW. To better understand the influence of FW particles, its aging
556 processes after emission were analyzed. It should be emphasized that during SF, contributions
557 from other human sources were low (Fig.9), so the air quality in these days was mainly influenced
558 by the highest contributor-FW particles' aging processes, including deposition, dispersion and
559 transformations.

560 From Fig.2b and Fig.10b, it can be seen that it takes about four days for the highest PM_{2.5} and
561 FW tracers-Ba and Sr on CNY to step down to the normal values of pre-CNY. The same situations
562 were found for K⁺, Cl⁻, NH₄⁺ and NO₃⁻ (Fig.11a). For SO₄²⁻, on Feb.3, its mass concentrations
563 decreased to a lower level of 6.1 μg m⁻³. Then on Feb.4, it did not decrease immediately to the
564 level of Jan. 29 until a rainfall (9 mm) on Feb.5. New emissions related with scattered fireworks
565 burning at surroundings were thought to be introduced on Feb.4 as Ba, Sr, K⁺, Ca²⁺, Ca and Na⁺
566 (they are all from primary emissions) slightly increased on Feb.4. Therefore, the variations of
567 SO₄²⁻ on Feb.5 may not just related with the aging of the intensive FW particles at CNY's Eve. On
568 Feb.1, though PM_{2.5} has decreased from 317 to 185 μg m⁻³, the visibility was still low as 2.2 km,
569 with peak concentrations of NH₄⁺, NO₃⁻ and SO₄²⁻ (they contributed 65% to the b_{ext}). On Feb.3,
570 PM_{2.5} decreased to 30 μg m⁻³, haze pollution still existed with the visibility as 6.7 km, mainly
571 contributed by ammonium sulfate (67%). It can be preliminarily concluded that the intensive FW
572 particles at CNY's Eve can influence the air quality for about four days by changing the main
573 contributors of extinction coefficient from EC+OM to ammonium sulfate. Drewnick et al. (2006)
574 also found that after about three or four days, the aerosol mass concentrations dropped to about
575 one-third of the concentrations for Near Year's firework burning period, while the relative
576 compositions of aerosols for the two periods were similar. And the mass concentrations of nitrate,
577 sulfate and ammonium increased again after about three days.

578

579

(Fig.11)

580

581 Pollution gases (SO₂, NO_x, etc.) emitted during FW events may be oxidized to secondary
582 organic and inorganic components that may be adsorbed onto particles (Sarkar et al., 2010). From
583 Fig.11a, we can find that Ca²⁺, NH₄⁺, NO₃⁻ and SO₄²⁻ showed peak values on CNY and two days
584 after, suggesting the directly emission from FW and secondary formations through heterogeneous
585 reactions of SO₂ and NO_x on crustal materials. Higher correlations were found for NO₃⁻-Ca²⁺
586 (R²=0.64) and SO₄²⁻-Ca²⁺ (R²=0.70). The lower wind speed (1.7-2.6 m s⁻¹) and mixing layer
587 heights (257-284 m) helped to capture pollution gases near the ground and higher RH (74%-88%)
588 favored their secondary transformation and following condensation onto pre-existing aerosols at
589 the initial four days after intensive FW emissions on CNY.

590 From Jan. 30 to Feb. 4, the ratios of soot-EC/NO₃⁻, Cl⁻/K⁺, NO₃⁻/SO₄²⁻ and Ca²⁺ decreased
591 first and then increased again, while to the opposite for SO₄²⁻/K⁺, suggesting the secondary
592 formation (Fig.11b). Secondary formations of NH₄⁺, NO₃⁻ and SO₄²⁻ from the gases emitted from
593 FW were also found in other cities (Wang et al., 2007; Yang et al., 2014). During aging, the direct
594 emission of KCl from fireworks (Drewnick et al., 2006) (R²=0.85 for K⁺-Cl⁻) can react with
595 H₂SO₄ and HNO₃ to form SO₄²⁻ (R²=0.76 for K⁺-SO₄²⁻) and NO₃⁻ (R²=0.96 for K⁺-NO₃⁻), leading
596 to the decreasing of Cl⁻/K⁺ ratio and increasing of SO₄²⁻/K⁺ ratio. Li et al. (2013) drew the same
597 conclusion through single particle analysis as that K-rich particles containing significant amounts
598 of S in the form of K₂SO₄ at a background site under the influence of FW. It implied the existence
599 of the aging of fresh FW particles via heterogeneous reactions during long-range transport. Soot
600 (soot-EC) can be directly introduced by firework displays (Do et al., 2012) which showed
601 moderate correlations with NO₃⁻ and SO₄²⁻ (R²=0.47 and 0.56, respectively) in this study,
602 indicating the coating of NO₃⁻ and SO₄²⁻ on soot. The OC/EC ratio peaked on CNY (as 6.8) which
603 was mainly contributed by the increasing of OC1, OC2 and OPC. They are related with
604 volatilization of the organic materials used for fireworks producing. The smelting point
605 temperatures for polyvinyl alcohol, polyoxyethylene and shell-lac are 230-240°C, 212°C,
606 115-120°C and the softening point for phenol formaldehyde resin is 80-85°C, all lower than the
607 detecting temperature for OC2 (230°C). Therefore, OC1, OC2 and OPC are more easily and

608 directly emitted from FW. The initially decreasing OC/EC ratio indicated the gradual formation
609 of secondary (aged) organic aerosols (Feng et al., 2012). To summarize, the heterogeneous
610 reactions of SO₂ and NO_x on crustal materials directly from FW, the replacement of Cl⁻ by NO₃⁻
611 and SO₄²⁻, coating of NO₃⁻ and SO₄²⁻ on soot and formation of secondary organic aerosols are the
612 main aging mechanisms of FW particles.

613 Previous studies also indicated that metals like Fe, Cu and Mn can catalyze the formation of
614 NO₃⁻ and SO₄²⁻ (Wang et al., 2007; Do et al., 2012; Feng et al., 2012). Wang et al. (2007)
615 indicated that the heterogeneous formation of sulfate through reacting with α-Fe₂O₃ existed under
616 moist atmosphere and was a function of RH and HNO₃. As shown in Fig.12 and Supplementary
617 file S9, significant correlations are found between NO₃⁻ and Fe, Cu and Mn and between SO₄²⁻ and
618 Fe, Cu and Mn at higher RH. It indicated the mechanism of metal-catalyzed formation of NO₃⁻
619 and SO₄²⁻ was more likely to occur at higher RH. On the day of CNY and Feb.2, the RH was 88%
620 and 87%, implying the occurrence of metal-catalyzed reactions, which may also explain the higher
621 NO₃⁻ and SO₄²⁻ concentrations at these days. The R² increased with the elevated RH. There are
622 obvious increases of R² for Fe-NO₃⁻, Mn-NO₃⁻ and Cu-NO₃⁻ when RH were >85%, >85%
623 and >65%, respectively. For the correlations of Fe-SO₄²⁻, Mn-SO₄²⁻ and Cu-SO₄²⁻, clear
624 increases in R² were found when RH were >85%, >85% and >55%. Then we can conclude that
625 for Fe-catalyzed and Mn-catalyzed reactions, the threshold of RH was around 85%; for
626 Cu-catalyzed formation of NO₃⁻ and SO₄²⁻, the thresholds of RH were around 65% and 55%,
627 respectively. For RH higher than 90%, R² decreased for Fe-NO₃⁻, Cu-NO₃⁻, Fe-SO₄²⁻ and
628 Mn-SO₄²⁻ which needs more data in the future to be verified and explained.

629

630 (Fig.12)

631

632 3.4.2 Potential health risks during the aging of fireworks burning particles

633 After they are emitted from the intensive FW at CNY's Eve, heavy metals including Vi, Cr,
634 Mn, Co, Ni, Cu, Zn, As, Cd and Pb decreased directly in the following four days (Supplementary
635 file S10). It indicated that they were emitted from FW primarily and were removed mainly by
636 dispersion and deposition during aging. Then we can assume that: (1) other emission sources (coal
637 combustion, vehicle exhaust and industrial processes were their main sources) for these metals

638 were stable during SF period; (2) the highest concentrations of them were just the combinations of
639 particles from the FW on Jan. 30 and other sources on Jan. 29. We subtract the concentrations of
640 elements on Jan. 29 from the corresponding values on Jan.30, Jan.31, Feb.1 and Feb.2 for each
641 element, respectively, to obtain the element concentrations just related with the FW particles.
642 Considering the variations of mixing layer height (as 306, 257, 227, 284 and 248 m for the five
643 days of Jan.29-Feb.2) and accumulation effect, the concentrations of these elements on Jan. 30,
644 Jan.31, Feb.1 and Feb.2 were transferred by factors of 0.84, 0.74, 0.93 and 0.81, respectively.
645 Then the $C_{95\%UCL}$ values raised by FW particles were 7.4, 21.2, 12.0, 23.7, 0.42, 5.2, 54.5, 11.7,
646 126 and 837 ng m^{-3} of the ten elements, respectively, for the four days. The non-cancer risks
647 raised just by FW particles at CNY's Eve were below 1 (0.03 and 0.02 for children and adult)
648 (Fig.13), indicating no adverse health effects. However the cancer risk was 1.62×10^{-6} , higher than
649 10^{-6} , suggesting the FW particles were important carcinogens and should be controlled effectively
650 especially for the contained Cd and As. Meanwhile, the risk level for children was higher than that
651 for adult, which meant that children were more sensitive to non-carcinogenic effects and should be
652 kept from possible exposure to them (Yang et al., 2014). The FW should be restricted at SF from
653 the view of their cancer risks to human health.

654
655 (Fig.13)
656

657 4 Conclusions

658 Thirty-nine elements, ten water-soluble ions and eight fractions of carbonaceous species were
659 measured to fully characterize the chemical compositions in atmospheric $\text{PM}_{2.5}$ in Nanjing during
660 the 2014 Chinese Spring Festival (SF). Serious regional haze pollution occurred and lasted during
661 the whole sampling period. At the Chinese New Year (CNY)'s Eve, after it peaked at 02:00, $\text{PM}_{2.5}$
662 exponentially decreased in the following 11 hours to the level before extensive fireworks burning
663 (FW) activities. Due to holiday effect, almost all elements decreased during SF except for Al, K, Ba
664 and Sr which were related with FW. As the "spring travel rush" effect, NO_3^- , OC and EC showed
665 highest values for periods before SF, indicating the extremely high traffic flows. At the New
666 Year's Eve, about 60.1% of the $\text{PM}_{2.5}$ mass was estimated to be from FW. Highly elevated Ba and
667 Sr were also found (highly correlated with each other), indicating they can be used as the tracers

668 of FW. The intensive FW at CNY's Eve obviously changed the chemical compositions of PM_{2.5},
669 with elevated organic matter (OM) immediately, contributing 39.3% of PM_{2.5}. The contributions
670 of secondary ions formed by gas-particle transformations gradually increased during FW particles'
671 aging processes. After FW particles emitted on CNY, the contribution of (NH₄)₂SO₄ to extinction
672 coefficient increased from 36% to 67%; while for NH₄NO₃ and EC, their contributions increased
673 first and then decreased. According to tracers and principle component analysis, fireworks burning
674 was the most important source of PM_{2.5} at this site. They contributed about half of PM_{2.5} during
675 SF. Tracers for various sources (As and Sb for coal combustion, Ba and Sr for FW, OC and EC for
676 vehicle emission, Ca for construction or road dust, Na⁺ for sea salt and Li, Be and Si for soil)
677 performed well and they varied accordantly with the contributions of corresponding sources. The
678 FW particles emitted from CNY's Eve may undergo about four days' aging processes from the
679 variations of Ba, Sr, NH₄⁺, NO₃⁻, SO₄²⁻ and K⁺. The aging processes were characterized by
680 heterogeneous reactions of SO₂ and NO_x on crustal materials directly from FW, the replacement of
681 Cl⁻ by NO₃⁻ and SO₄²⁻, coating of NO₃⁻ and SO₄²⁻ on soot, formation of secondary organic aerosols
682 and metal-catalyzed formation of NO₃⁻ and SO₄²⁻ at higher relative humidity. For Fe-catalyzed and
683 Mn-catalyzed reactions, the thresholds of RH were around 85%; while for Cu-catalyzed formations
684 of NO₃⁻ and SO₄²⁻, the thresholds of RH were around 65% and 55%, respectively. During the
685 aging processes, FW particles on CNY obviously changed the main contributors to the extinction
686 coefficient from EC+OM to ammonium sulfate. Meanwhile, higher cancer risks raised by heavy
687 metals (especially for Cd and As) only related with FW particles emitted at CNY's Eve was
688 1.62×10^{-6} , which also imposed higher non-cancer risks to children than adult. The results in this
689 study will be useful for understanding the detailed compositions and aging processes of FW
690 particles and also highlight the importance of controlling intensive fireworks burning in order to
691 protect air quality and reduce the cancer risks.

692

693 **Acknowledgment.** This work was funded by the National Natural Sciences Foundation of China
694 (No. 41030962), Scientific and technological cooperation between the Government of
695 China-Serbia (2013(158)2-10), the grant of China Scholarship Council and the Priority Academic
696 Program Development (PAPD) of Jiangsu Higher Education Institution.

697

698 **References**

- 699 Allan, J. D., Williams, P. I., Morgan, W. T., Martin, C. L., Flynn, M. J., Lee, J., Nemitz, E.,
700 Phillips, G. J., Gallagher, M.W., and Coe, H.: Contributions from transport, solid fuel
701 burning and cooking to primary organic aerosols in two UK cities, *Atmos. Chem. Phys.*, 10,
702 647-668, doi:10.5194/acp-10-647-2010, 2010.
- 703 Attri, A. K., Kumar, U., and Jain, V. K.: Microclimate: formation of ozone by fireworks, *Nature*,
704 411, 1015, 2001.
- 705 **Baptistaa, L.F., and Miguel, E. D.: Geochemistry and risk assessment of street dust in Luanda,**
706 **Angola: A tropical urban environment, *Atmos. Environ.*, 39, 4501-4512, 2005.**
- 707 Cao, J. J., Wu, F., Chow, J. C., Lee, S. C., Li, Y., Chen, S.W., An, Z. S., Fung, K. K., Watson, J.
708 G., Zhu, C. S., and Liu, S. X.: Characterization and source apportionment of atmospheric
709 organic and elemental carbon during fall and winter of 2003 in Xi'an, China, *Atmos. Chem.*
710 *Phys.*, 5, 3127-3137, doi:10.5194/acp-5-3127-2005, 2005.
- 711 Deka, P., and Hoque, R.R.: Incremental effect of festive biomass burning on wintertime PM₁₀ in
712 Brahmaputra Valley of Northeast India, *Atmos. Res.*, 143, 380-391, 2014.
- 713 Do, T. M., Wang, C.F., Hsieh, Y. K., and Hsieh, H. F.: Metals Present in Ambient Air before and
714 after a Firework Festival in Yanshui, Tainan, Taiwan, *Aerosol Air Qual. Res.*, 12, 981-993,
715 2012.
- 716 Drewnick, F., Hings, S. S., Curtius, J., Eerdekens, G., and Williams, J.: Measurement of
717 fine particulate and gas-phase species during the New Year's Fireworks 2005 in Mainz,
718 Germany, *Atmos. Environ.*, 40, 4316-4326, 2006.
- 719 Dutschke, A., Lohrer, C., Kurth, L., Seeger, S., Barthel, M., and Panne, U.: Aerosol Emissions
720 from Outdoor Firework Displays. *Chem. Eng. Technol.*, 12, 2044-2050, 2011.
- 721 Estrellan, C. R., and Iino, F.: Toxic emissions from open burning, *Chemosphere*, 80, 193-207,
722 2010.
- 723 Feng, J. L., Sun, P., Hu, X. L., Zhao, W., Wu, M. H., and Fu, J. M.: The chemical composition and
724 sources of PM_{2.5} during the 2009 Chinese New Year's holiday in Shanghai, *Atmos. Res.*, 118,
725 435-444, 2012.
- 726 Godri, K. J., Green, D. C., Fuller, G. W., OSTO, M. D., Beddows, D. C., Kelly, F. J., Harrison, R.
727 M., and Mudway, I. S.: Particulate Oxidative Burden Associated with Firework Activity,
728 *Environ. Sci. Technol.*, 44, 8295-8301, 2010.
- 729 **Granero, S., and Domingo, J.: Levels of metals in soils of Alcala de Henares, Spain: Human health**
730 **risks, *Environ. Int.*, 28, 159-164, 2002.**
- 731 Han, Y. M., Cao, J. J., Lee, S. C., Ho, K. F., and An, Z. S.: Different characteristics of char and
732 soot in the atmosphere and their ratio as an indicator for source identification in Xi'an, China,
733 *Atmos. Chem. Phys.*, 10, 595-607, doi:10.5194/acp-10-595-2010, 2010.
- 734 Han, Y. M., Han, Z. W., Cao, J. J., Chow, J. C., Watson, J. G., An, Z. S., Liu, S. X., and Zhang, R.
735 J.: Distribution and origin of carbonaceous aerosol over a rural high-mountain lake area,
736 Northern China and its transport significance, *Atmos. Environ.*, 42, 2405-2414, 2008.
- 737 Huang, K., Zhuang, G.S., Lin, Y., Wang, Q., Fu, J. S., Zhang, R., Li, Deng, J. C., and Fu, Q.Y.:
738 Impact of anthropogenic emission on air quality over a megacity-revealed from an intensive
739 atmospheric campaign during the Chinese Spring Festival, *Atmos. Chem. Phys.*, 12,
740 11631-11645, doi:10.5194/acp-12-11631-2012, 2012.
- 741 Jiang, Q., Sun, Y. L., Wang, Z., and Yin, Y.: Aerosol composition and sources during the Chinese

742 Spring Festival: fireworks, secondary aerosol, and holiday effects, *Atmos. Chem. Phys.*
743 *Discuss.*, 14, 20617-20646, doi:10.5194/acpd-14-20617-2014, 2014.

744 Jing, H., Li, Y. F., Zhao, J.T., Li, B., Sun, J. L., Chen, R. Gao, Y. X., and Chen, C. Y.: Wide-range
745 particle characterization and elemental concentration in Beijing aerosol during the 2013
746 Spring Festival, *Environ. Pollut.*, 192, 204-211, 2014.

747 Joly, A., Smargiassi, A., Kosatsky, T., Fournier, M., Dabek-Zlotorzynska, E., Celso, V., Mathieu,
748 D., Servranckx, R., D'amours, R., Malo, A., and Brook, J.: Characterisation of particulate
749 exposure during fireworks displays, *Atmos. Environ.*, 44, 4325-4329, 2010.

750 Kang, H. Q., Zhu, B., Su, J. F., Wang, H. L., Zhang, Q. C., and Wang, F.: Analysis of a
751 long-lasting haze episode in Nanjing, China, *Atmos. Res.*, 120-121, 78-87, 2013.

752 Kim, K. W., Kim, Y. J., Oh, S. J.: Visibility impairment during Yellow Sand periods in the urban
753 atmosphere of Kwangju, Korea, *Atmos. Environ.*, 35, 5157-5167, 2001.

754 Kong, S. F., Ji, Y. Q., Lu, B., Zhao, X. Y., Chen, L., Bai, Z. P., Xu, Y. H., Liu, Y., and Jiang, H.:
755 Characteristic of PM_{2.5}, PM₁₀ and TSP source profiles for fugitive dust in a coastal oilfield
756 city, China, *Aerosol Air Qual. Res.*, 14, 2017-2028, 2014a.

757 Kong, S. F., Wen, B., Chen, K., Yin, Y., Li, Q., Li, L., Yuan, L., and Sun, X.: Ion chemistry for
758 atmospheric size-segregated aerosol and depositions at an offshore site of Yangtze River
759 Delta (YRD) region, China, *Atmos. Res.*, 147-148, 205-226, 2014b.

760 Kong, S. F., Han, B., Bai, Z. P., Chen, L., Shi, J. W., and Xu, Z.: Receptor modeling of PM_{2.5},
761 PM₁₀ and TSP in different seasons and long-range transport analysis at a coastal site of
762 Tianjin, China, *Sci. Total Environ.*, 408, 4681-4694, 2010.

763 Kong, S. F., Lu, B., Ji, Y. Q., Zhao, X. Y., Bai, Z. P., Xu, Y. H., Liu, Y., and Jiang, H.: Risk
764 assessment of heavy metals in road and soil dust within PM_{2.5}, PM₁₀ and PM₁₀₀ fractions in
765 Dongying city, Shandong Province, China, *J. Environ. Monito.*, 14, 791-803, 2012.

766 Li, L., Yin, Y., Kong, S. F., Wen, B., Chen, K., Yuan, L., and Li, Q.: Altitudinal effect to the size
767 distribution of water soluble inorganic ions in PM at Huangshan, China, *Atmos. Environ.*, 98,
768 242-252, 2014.

769 Li, M. N., and Zhang, L.: Haze in China: Current and future challenges, *Environ. Pollut.*, 189,
770 85-86, 2014.

771 Li, P. H., Han, B., Huo, J., Lu, B., Ding, X., Chen, L., Kong, S. F., Bai, Z. P., and Wang, B.:
772 Characterization, meteorological influences and source identification of carbonaceous aerosol
773 during autumn-winter period in Tianjin, China, *Aerosol Air Qual. Res.*, 2, 283-294, 2012.

774 Li, W. J., Shi, Z. B., Yan, C., Yang, L. X., Dong, C., and Wang, W. X.: Individual metal-bearing
775 particles in a regional haze caused by firecracker and firework emissions, *Sci. Total Environ.*,
776 443, 464-469, 2013.

777 Moreno, T., Querol, X., Alastuey, A., Minguillón, M. C., Pey, J., Rodriguez, S., Miró, J. V., Felis,
778 C., and Gibbons, W.: Recreational atmospheric pollution episodes: Inhalable metalliferous
779 particles from firework displays, *Atmos. Environ.*, 41, 913-922, 2007.

780 Richard, A., Gianini, M. F. D., Mohr, C., Furger, M., Bukowiecki, N., Minguillón, M. C.,
781 Lienemann, P., Flechsig, U., Appel, K., DeCarlo, P. F., Heringa, M. F., Chirico, R.,
782 Baltensperger, U., and Prévôt, A. S. H.: Source apportionment of size and time resolved trace
783 elements and organic aerosols from an urban courtyard site in Switzerland, *Atmos. Chem.*
784 *Phys.*, 11, 8945-8963, doi:10.5194/acp-11-8945-2011, 2011.

785 Sarkar, S., Khillare, P. S., Jyethi, D. S., Hasan, A., and Parween, M.: Chemical speciation of

786 respirable suspended particulate matter during a major firework festival in India, *J. Hazard.*
787 *Mater.*, 184, 321-330, 2010.

788 Shen, Z. X., Cao, J. J., Arimoto, R., Han, Z. W., Zhang, R. J., Han, Y. M., Liu, S. X., Okuda, T.,
789 Nakao, S., and Tanaka, S.: Ionic composition of TSP and PM_{2.5} during dust storms and air
790 pollution episodes at Xi'an, China, *Atmos. Environ.*, 43, 2911-2918, 2009.

791 Tan, P. H., Chou, C., Liang, J. Y., Chou, C. C. K., and Shiu, C. J.: Air pollution "holiday effect"
792 resulting from the Chinese New Year, *Atmos. Environ.*, 43, 2114-2124, 2009.

793 Tao, J., Ho, K. F., Chen, L. G., Zhu, L. H., Han, J. L., Xu, Z. C.: Effect of chemical composition of
794 PM_{2.5} on visibility in Guangzhou, China, 2007 spring. *Particuology*, 7, 68-75, 2009.

795 Terzi, E., Argyropoulos, G., Bougatioti, A., Mihalopoulos, N., Nikolaou, K., and Samara, C.:
796 Chemical composition and mass closure of ambient PM₁₀ at urban sites, *Atmos. Environ.*, 44,
797 2231-2239, 2010.

798 Tian, Y. Z., Wang, J., Peng, X., Shi, G. L., and Feng, Y. C.: Estimation of direct and indirect
799 impacts of fireworks on the physicochemical characteristics of atmospheric fine and coarse
800 particles, *Atmos. Chem. Phys.*, 14, 9469-9479, doi:10.5194/acp-14-9469-2014, 2014.

801 Tsai, H. H., Chien, L. H., Yuan, C. S., Lin, Y. C., Jen, Y. H., and Ie, I. R.: Influences of fireworks
802 on chemical characteristics of atmospheric fine and coarse particles during Taiwan's Lantern
803 Festival, *Atmos. Environ.*, 62, 256-264, 2012.

804 Tsyro, S. G.: To what extent can aerosol water explain the discrepancy between model calculated
805 and gravimetric PM₁₀ and PM_{2.5}, *Atmos. Chem. Phys.*, 5, 515-532, 2005.

806 Vecchi, R., Bernardoni, V., Cricchio, D., Alessandro, A. D., Fermo, P., Lucarelli, F., Nava, S.,
807 Piazzalunga, A., and Valli, G.: The impact of fireworks on airborne particles. *Atmos.*
808 *Environ.*, 42, 1121-1132, 2008.

809 Wang, H. L., An, J. L., Shen, L. J., Zhu, B., Pan, C., Liu, Z. R., Liu, X. H., Duan, Q., Liu, X.,
810 Wang, Y. S.: Mechanism for the formation and microphysical characteristics of submicron
811 aerosol during heavy haze pollution episode in the Yangtze River Delta, China, *Sci. Total*
812 *Environ.*, 490, 501-508, 2014.

813 Wang, Q. Y., Cao, J. J., Shen, Z. X., Tao, J., Xiao, S., Luo, L., He, Q. Y., and Tang, X. Y.:
814 Chemical characteristics of PM_{2.5} during dust storms and air pollution events in Chengdu,
815 China, *Particuology* 11, 70-77, 2013.

816 Wang, Y., Zhuang, G. S., Xu, C., and An, Z. S.: The air pollution caused by the burning of
817 fireworks during the lantern festival in Beijing, *Atmos. Environ.*, 41, 417-431, 2007.

818 Wehner, B., Wiedensohler, A., and Heintzenberg, J.: Submicrometer aerosol size distribution and
819 mass concentration of the millennium fireworks 2000 in Leipzig, Germany, *J. Aerosol Sci.*,
820 12, 1489-1493, 2000.

821 Williams, J., Drewnick, F., Hings, S.S., Curtius, J., Eerdekens, G., Klüpfel, T., and Wagner, T.:
822 Firework emissions for Satellite Validation? *Environ. Chem.*, 2, 94-95, 2005.

823 Yang, L. X., Gao, X. M., Wang, X. F., Nie, W., Wang, J., Gao, R., Xu, P. J., Shou, Y. P., Zhang,
824 Q. Z., and Wang, W. X.: Impacts of firecracker burning on aerosol chemical characteristics
825 and human health risk levels during the Chinese New Year Celebration in Jinan, China, *Sci.*
826 *Total Environ.*, 476-477, 57-64, 2014.

827 Yang, L. X., Wang, D. C., Cheng, S. H., Wang, Z., Zhou, Y., Zhou, X. H., and Wang, W. X.:
828 Influence of meteorological conditions and particulate matter on visual range impairment in
829 Jinan, China, *Sci. Total Environ.*, 383, 164-173, 2007.

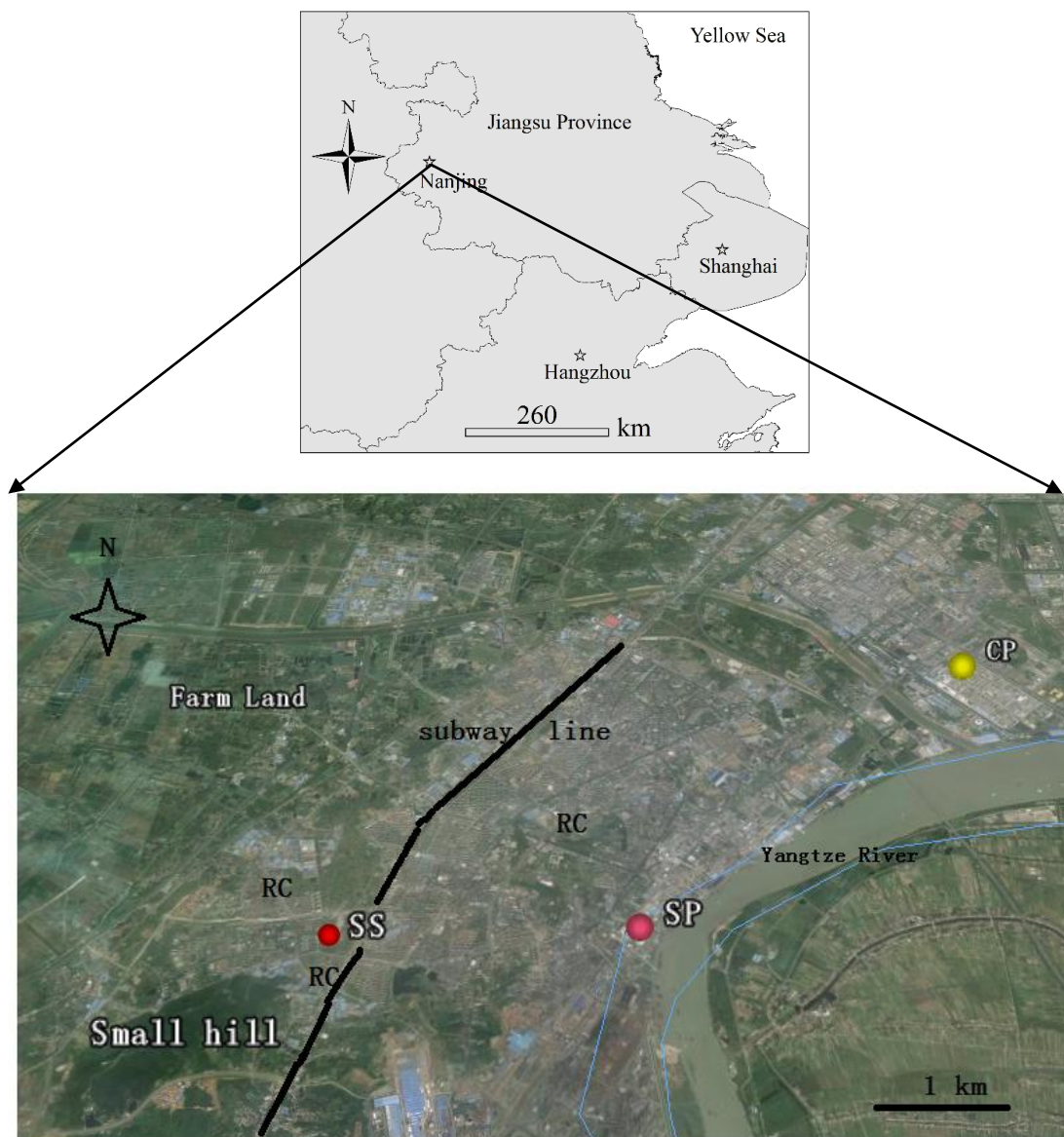
830 Ye, C., Chen, R. S., and Young, C.: Nian: when Chinese mythology affects air pollution, The
831 Lancet, 9935, 2125, 2014.

832 Yu, X. N., Shi, C. Z., Ma, J., Zhu, B., Li, M., Wang, J., Yang, S.Y., and Kang, N.: Aerosol optical
833 properties during firework, biomass burning and dust episodes in Beijing, Atmos. Environ.,
834 81. 475-484. 2013.

835 Zhang, M., Wang, X. M., Chen, J. M., Cheng, T. T., Wang, T., Yang, X., Gong, Y. G., Geng, F.
836 H., and Chen, C.H.: Physical characterization of aerosol particles during the Chinese New
837 Year's firework events, Atmos. Environ., 44, 5191-5198, 2010.

838
839
840
841
842
843
844
845
846
847
848
849
850
851
852
853
854
855
856
857
858
859
860
861
862
863
864
865
866
867
868
869
870
871
872
873

874



875

876 Fig. 1 Location of the sampling site (the red dot, SS). SP: iron smelt plant; CP: chemical industrial
877 park; RC: residential community. The black line indicates the subway line near SS.

878

879

880

881

882

883

884

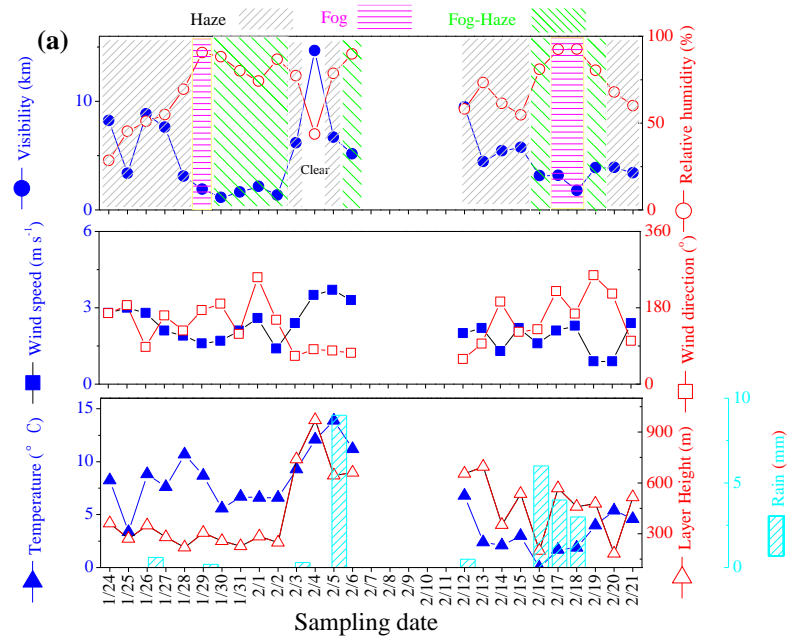
885

886

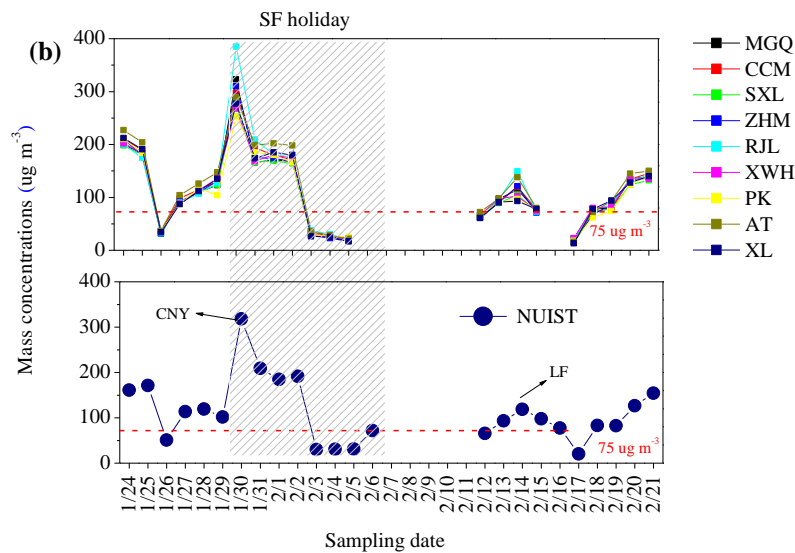
887

888

889



890



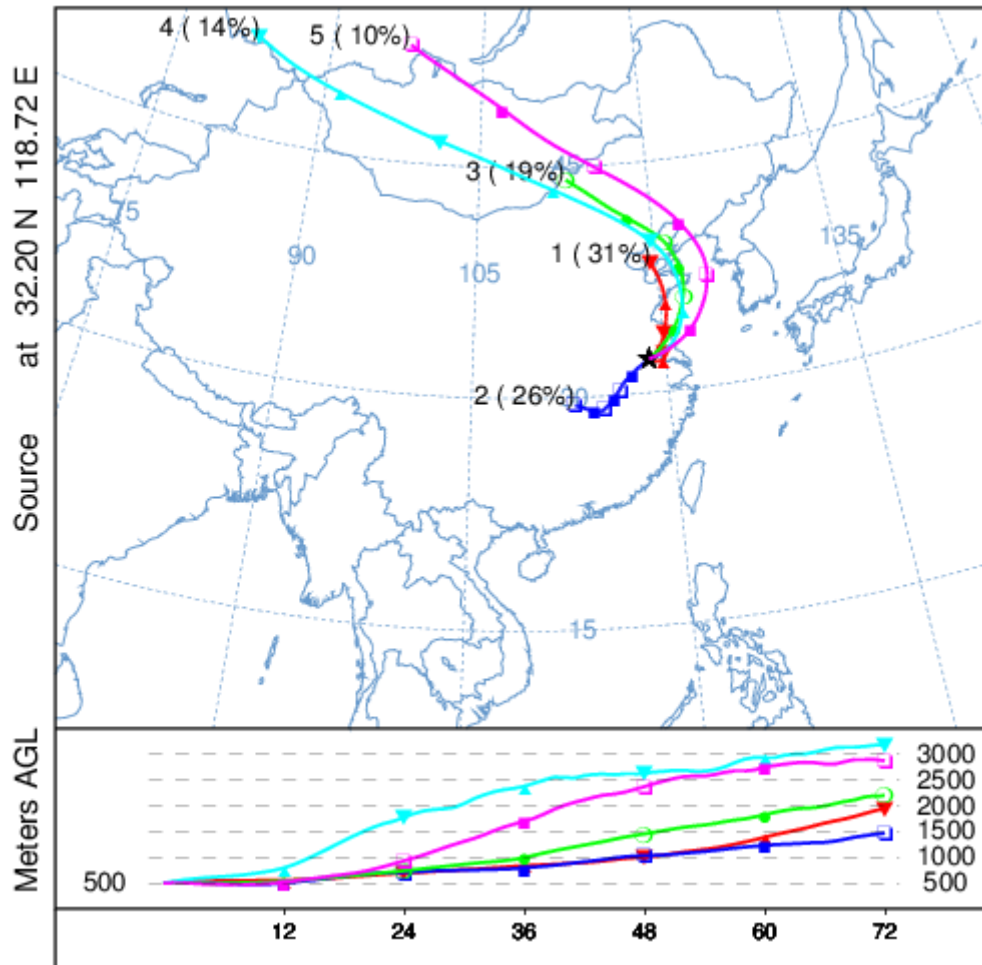
891

892 Fig.2 Daily variation of meteorological factors (a) and mass concentrations of PM_{2.5} (b) during
 893 sampling periods. MGQ, CCM, SXL, ZHM, RJL, XWH, PK, AT and XL indicate the nine urban
 894 air quality monitoring sites set by Jiangsu Environmental Monitoring Center as Supplementary file
 895 S4 shown. NUIST indicates the sampling site of this study at Nanjing University of Information
 896 Science and Technology. SF means Spring Festival (between Jan. 30-Feb.7); CNY means Chinese
 897 New Year day (Jan.30); LF means Lantern Festival day (Feb. 14). 75 $\mu\text{g m}^{-3}$ is the 24 h-averaged
 898 secondary standard value for PM_{2.5} of China National Ambient Air Quality.

899

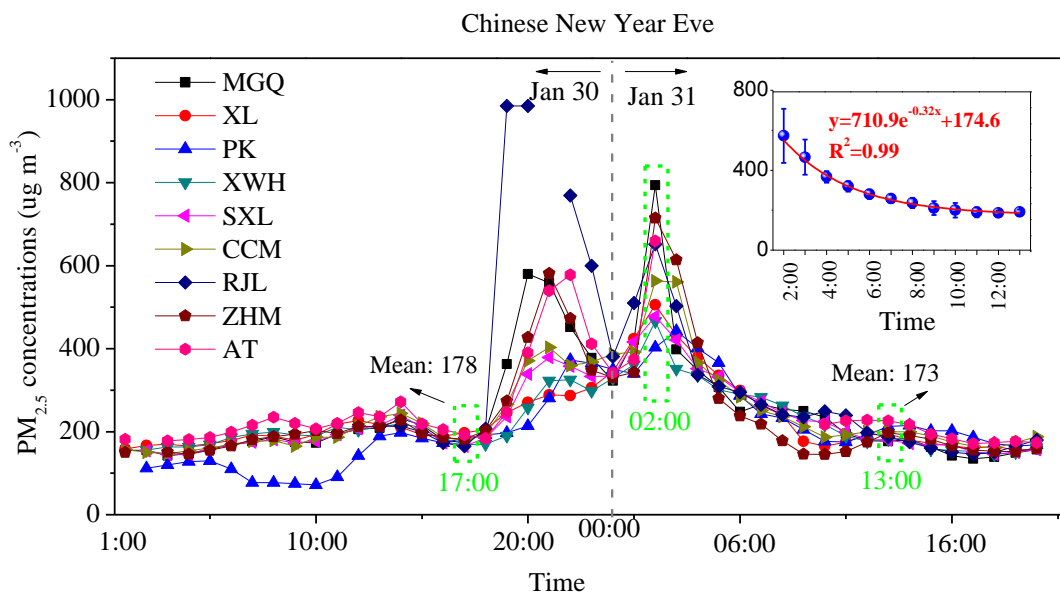
900

901



902 Fig.3 Cluster analysis for backward trajectories of air masses during the whole sampling periods.
 903 The different colors indicated different clusters of the backward trajectories.
 904

905
 906
 907
 908
 909
 910
 911
 912
 913
 914
 915
 916
 917
 918
 919



920

921 Fig.4 Hourly PM_{2.5} concentrations before, during and after Chinese New Year (CNY) Eve of
 922 2014 at Nanjing. The figure at the top-right corner indicates the decreasing trend of averaged
 923 PM_{2.5} mass concentrations after 02:00 of CNY Eve (on Jan. 30, 2014). Hourly data for the nine
 924 sites in urban Nanjing (locations were shown in supplementary file S4) were collected from the
 925 public platform at <http://218.94.78.75/jsair/>.

926

927

928

929

930

931

932

933

934

935

936

937

938

939

940

941

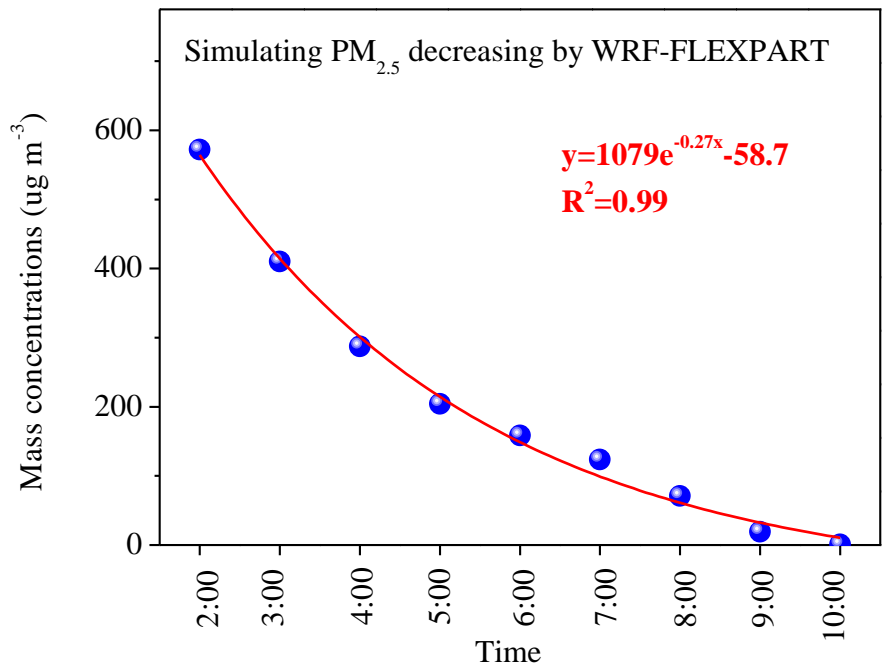
942

943

944

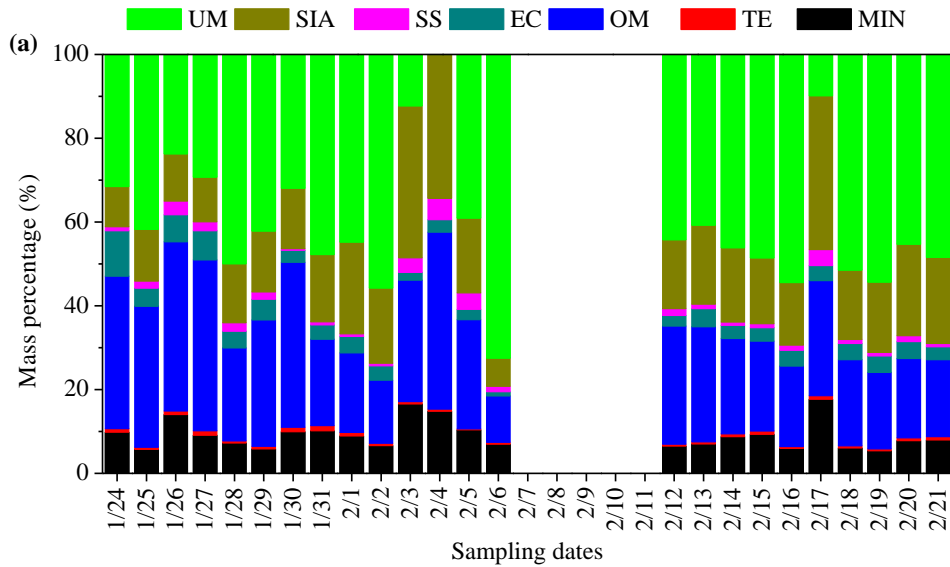
945

946

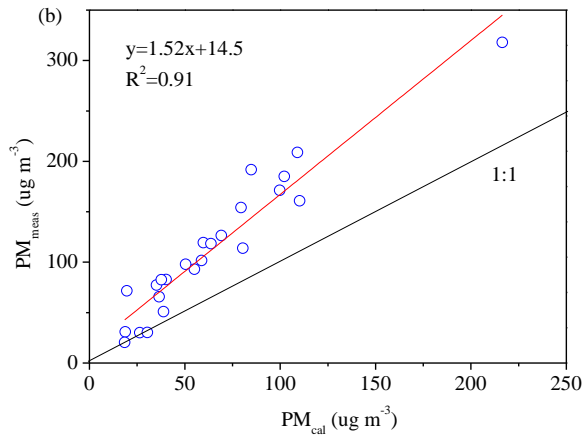


947
948
949
950
951
952
953
954
955
956
957
958
959
960
961
962
963
964
965
966
967

Fig.5 Particles decreasing trend at Chinese New Year’s Eve by WRF-FLEXPART simulating. The particle concentrations decreased to 0.76 $\mu\text{g m}^{-3}$ after nine hours, faster than the real decrease as Fig.4 shows. It can be explained as that we did not consider the injections of particles during simulating course, which biases the result.



968



969

970 Fig.6 Mass balance of chemical species in $PM_{2.5}$ at sampling periods (a) and relationship between
 971 the mass calculated by adding individual components and the gravimetrically measured particulate
 972 mass (b).

973 $MIN=2.14 \times Si+1.67 \times Ti+1.89 \times Al+1.59 \times Mn+1.67 \times Mg+1.95 \times Ca+1.35 \times Na+1.21 \times K+1.43 \times Fe$.

974 Trace elements (TE) indicated the sum of all other elements except for those used in calculating

975 MIN. Sea salt (SS)=[Na^+]+[ss-Cl⁻]+[ss-Mg²⁺]+[ss-K⁺]+[ss-Ca²⁺]+[ss-SO₄²⁻]; ss-Cl⁻=1.8×[Na⁺];

976 ss-Mg²⁺=0.12×[Na⁺]; ss-K⁺=0.036×[Na⁺]; ss-Ca²⁺=0.038×[Na⁺]; ss-SO₄²⁻=0.252×[Na⁺].

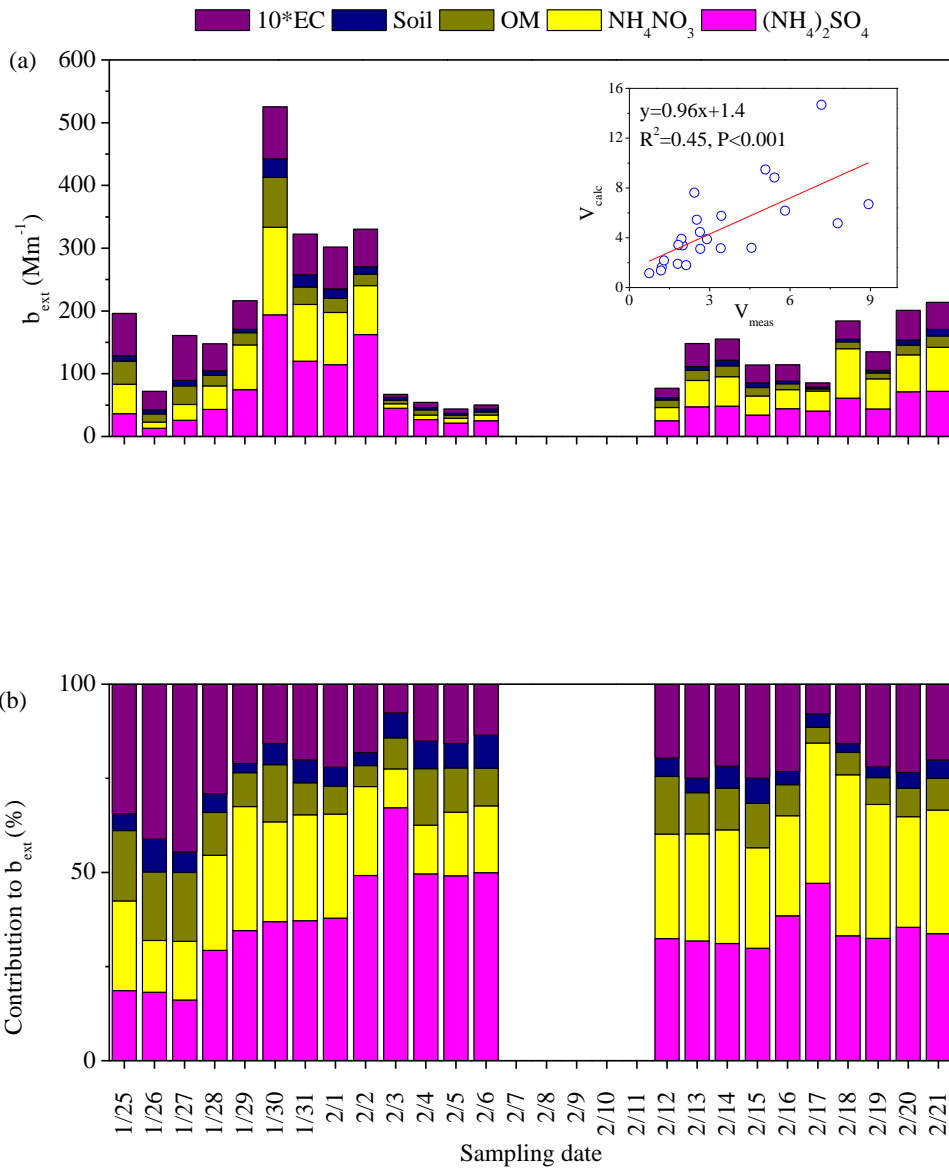
977 Secondary inorganic aerosol (SIA) was calculated as the sum of nss-SO₄²⁻, NO₃⁻ and NH₄⁺.

978 Organic matter (OM)=2.0×OC. UM indicated unidentified matter. Jan.30-Feb.7 belongs to the

979 Chinese Spring Festival in 2014; Jan. 30 is the Chinese New Year day; Feb. 14 is the Lantern
 980 Festival day.

981

982



983

984

985 Fig.7 Extinction coefficients of chemical components in $PM_{2.5}$ at Nanjing (a) and relative
 986 contribution to light extinction of chemical components in $PM_{2.5}$ (b). Jan. 30-Feb.7 belongs to the
 987 Chinese Spring Festival in 2014; Jan. 30 is the Chinese New Year day; Feb. 14 is the Lantern
 988 Festival day. V_{calc} indicates the visibility calculated by adding individual components; V_{meas} is the
 989 measured visibility.

990

991

992

993

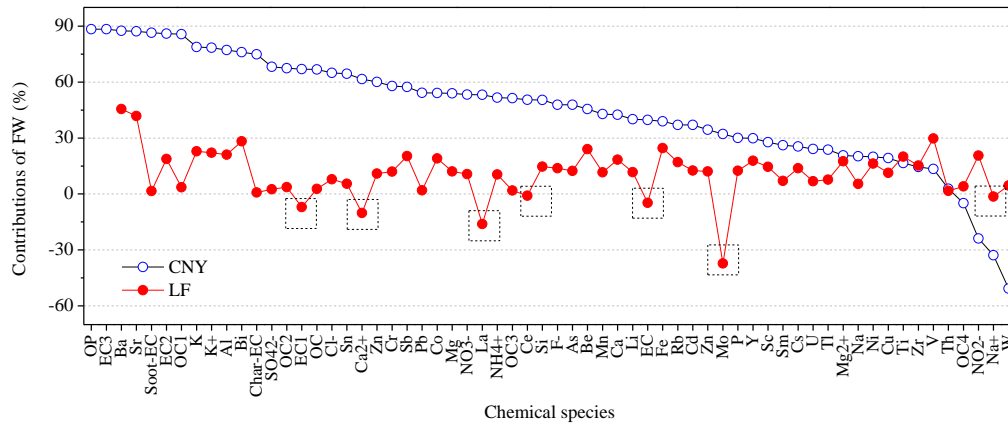
994

995

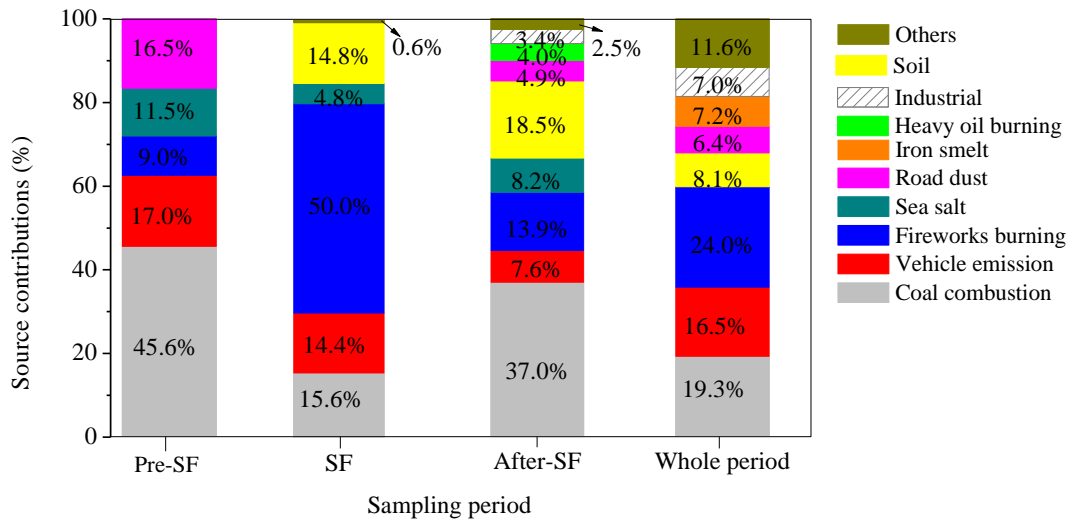
996

997

998



999
 1000 Fig.8 Contributions of fireworks burning (FW) on CNY and LF to chemical species in PM_{2.5}.
 1001 CNY means Chinese New Year day (Jan. 30); LF means Lantern Festival day (Feb. 14).
 1002
 1003
 1004
 1005
 1006
 1007
 1008
 1009
 1010
 1011
 1012
 1013
 1014
 1015
 1016
 1017
 1018
 1019
 1020
 1021
 1022



1023

1024 Fig.9 Source contributions to atmospheric PM_{2.5} before, during, after 2014 Spring Festival (SF)
 1025 and the whole period by principal component analysis. Pre-SF indicated the period before SF,
 1026 covering the days from Jan. 24 to Jan. 29; SF indicated the period during SF, covering the days
 1027 from Jan. 30 to Feb. 6; After-SF indicated the period after SF, covering the days from Feb.12 to
 1028 Feb.21. The whole period included Pre-SF, SF and After-SF period.

1029

1030

1031

1032

1033

1034

1035

1036

1037

1038

1039

1040

1041

1042

1043

1044

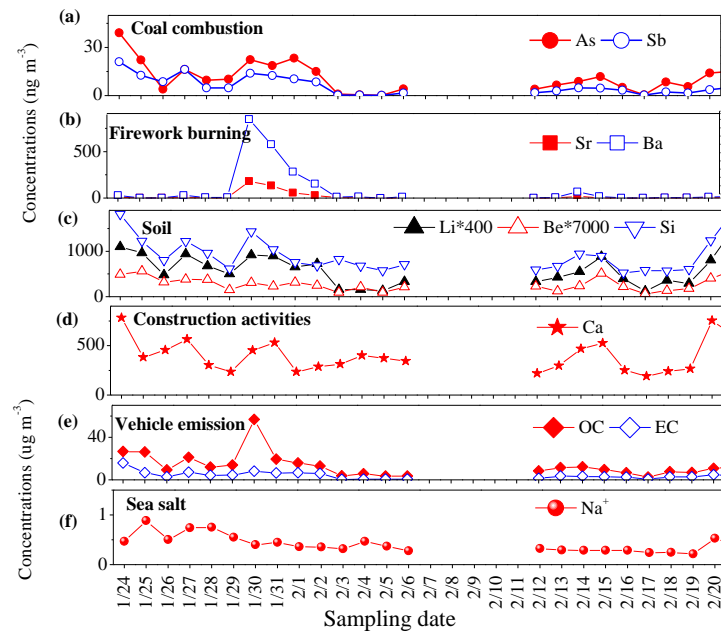
1045

1046

1047

1048

1049



1050

1051 Fig.10 Time series of tracers for (a) coal combustion, (b) fireworks burning, (c) soil,
 1052 construction activities or road dust, (e) vehicle emission and (f) sea salt. The Y-axis units for (a),
 1053 (b), (c) and (d) are ng m^{-3} and are ug m^{-3} for (e) and (f). Jan. 30-Feb.7 belongs to the Chinese
 1054 Spring Festival in 2014; Jan. 30 is the Chinese New Year day; Feb. 14 is the Lantern Festival day.

1055

1056

1057

1058

1059

1060

1061

1062

1063

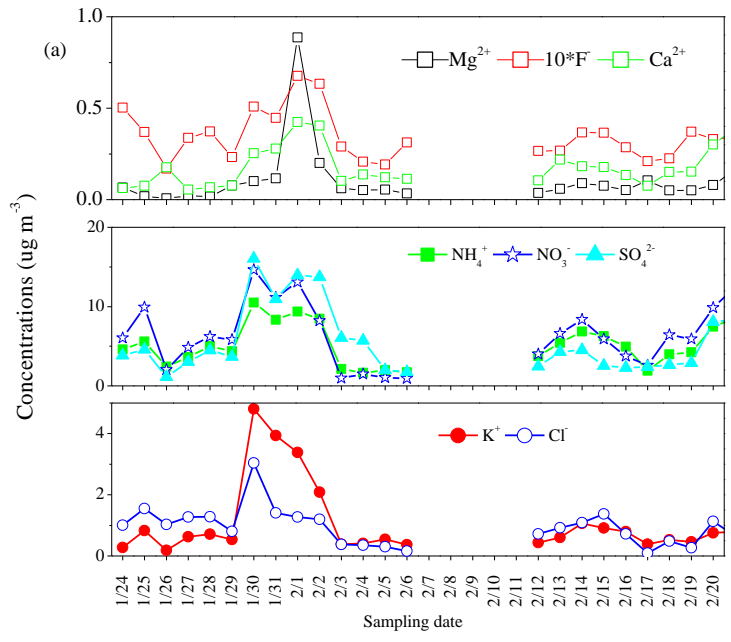
1064

1065

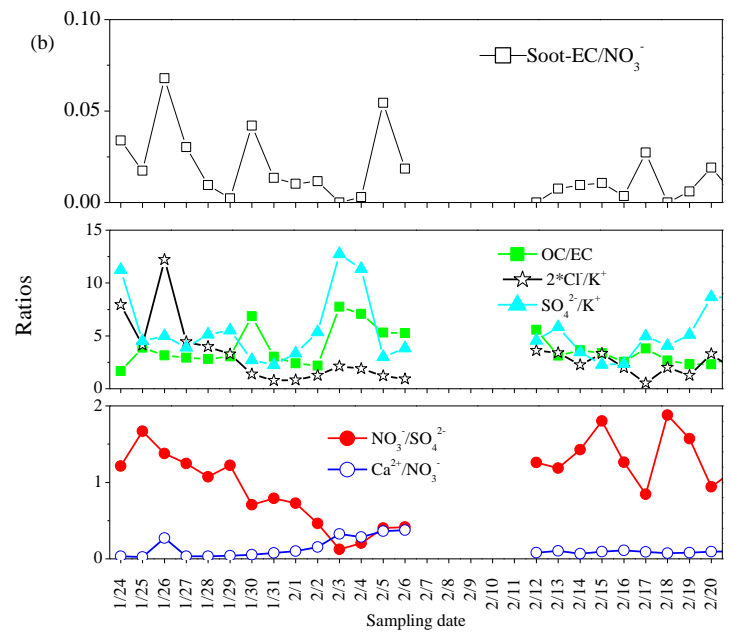
1066

1067

1068



1069



1070

1071 Fig.11 Time series of ions (a) and specific ratios (b) during sampling period. Jan. 30-Feb.7
 1072 belongs to the Chinese Spring Festival in 2014; Jan. 30 is the Chinese New Year day; Feb. 14 is
 1073 the Lantern Festival day.

1074

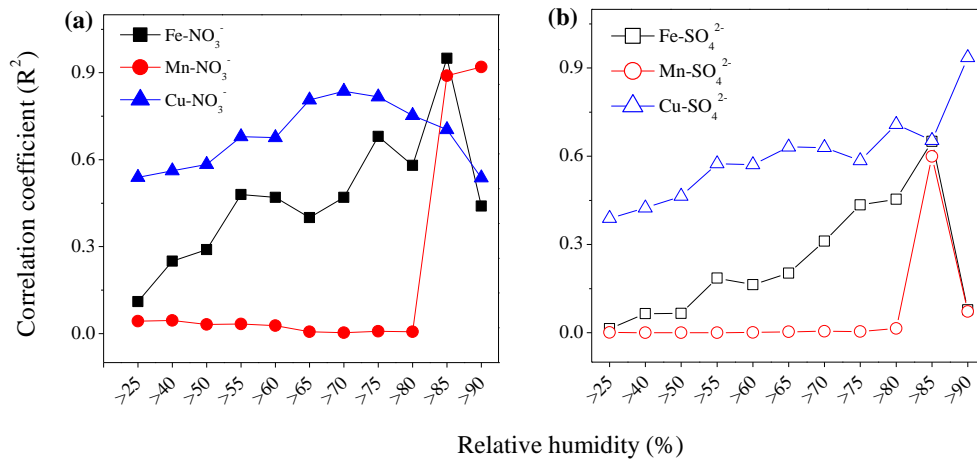
1075

1076

1077

1078

1079



1080

1081 Fig.12 Correlation coefficients (R^2) of NO_3^- and metals-Fe, Mn and Cu under certain relative
 1082 humidity bins (a); correlation coefficients of SO_4^{2-} and metals-Fe, Mn and Cu under certain
 1083 relative humidity bins (b). For each time of calculating the R^2 , the data of NO_3^- or SO_4^{2-} and each
 1084 metal were used for corresponding relative humidity bins.

1085

1086

1087

1088

1089

1090

1091

1092

1093

1094

1095

1096

1097

1098

1099

1100

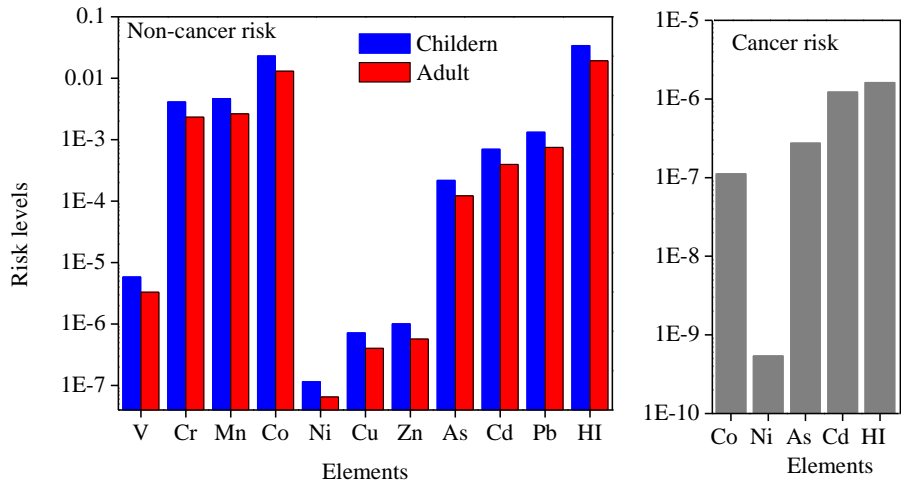
1101

1102

1103

1104

1105



1106

1107 Fig.13 Non-cancer and cancer risks for heavy metals raised by intensive fireworks burning at
 1108 Nanjing.

1109

1110

1111

1112

1113

1114

1115

1116

1117

1118

1119

1120

1121

1122

1123

1124

1125

1126

1127

1128

1129

1130

1131

1132

1133

1134

1135

1136 Table 1 Mass concentrations of elements in PM_{2.5} before, during and after 2014 Chinese Spring Festival at Nanjing (ng m⁻³)

Elements	Pre-SF	SF (without CNY)	After-SF (without LF)	CNY	LF	CNY/pre-CNY	LF/pre-LF
Li	1.9±0.7	1.1±0.8	1.4±1.0	2.3	1.4	1.8	1.3
Be	0.1±0.0	0.0±0.0	0.0±0.0	0.0	0.0	2.1	1.9
Na	826±209	417±196	435±172	563	506	1.3	1.1
Mg	124±79	97±89	106±30	196	124	2.6	1.3
Al	612±234	802±550	530±230	3127	811	7.9	1.7
Si	1105±420	752±147	847±422	1431	943	2.3	1.4
P	66±35	35±20	29±13	42	35	1.5	1.3
K	1940±725	3330±3848	1276±817	14336	2940	9.3	1.8
Ca	454±198	355±95	383±193	454	469	1.9	1.6
Sc	0.1±0.0	0.1±0.0	0.1±0.1	0.1	0.1	1.5	1.4
Ti	31±27	14±8	24±28	20	15	1.2	1.7
V	7.7±2.3	7.0±7.8	6.6±4.6	9.4	10.5	1.2	2.4
Cr	10.4±4.0	7.9±5.7	8.7±3.4	17.4	10.2	2.9	1.3
Mn	48±22	22±19	67±67	47	50	1.9	1.3
Fe	385±342	160±140	261±172	304	300	1.8	1.9
Co	0.4±0.1	0.4±0.4	0.4±0.2	0.6	0.5	2.6	1.6
Ni	8.5±6.0	4.5±3.1	8.9±5.6	5.9	7.6	1.3	1.5
Cu	102±30	81±63	77±25	170	116	1.3	1.3
Zn	257±145	93±81	194±154	242	174	1.6	1.3
As	17±13	9.0±9.8	8.0±4.6	22	8.8	2.2	1.3
Rb	8.5±2.2	4.7±4.2	5.7±4.5	12	6.5	1.7	1.5
Sr	5.1±3.9	34±49	4.9±5.9	181	20.5	79.4	5.7
Y	0.2±0.1	0.1±0.1	0.2±0.1	0.1	0.2	1.5	1.5
Zr	1.9±0.7	1.6±0.6	1.9±1.3	1.6	2.3	1.2	1.4

Mo	2.7±1.0	1.3±1.2	2.9±1.8	2.8	2.7	1.6	0.6
Cd	3.4±2.8	1.3±1.4	1.1±0.7	4.1	1.3	1.7	1.3
Sn	9.0±5.6	5.0±6.1	4.6±3.5	18.0	4.5	3.7	1.1
Sb	11±6.5	4.8±5.4	3.0±1.6	13.9	4.8	2.9	1.7
Cs	1.8±1.0	0.7±0.8	1.4±1.5	1.9	1.2	1.4	1.4
Ba	14±12	152±216	14.4±20.4	850	70.1	99.1	9.7
La	0.7±0.6	0.6±0.5	0.6±0.5	0.6	0.5	2.5	0.8
Ce	0.8±0.5	0.4±0.3	0.6±0.6	0.6	0.5	2.3	1.0
Sm	0.1±0.0	0.0±0.0	0.0±0.0	0.0	0.0	1.4	1.2
W	4.3±2.4	3.1±2.9	3.2±1.3	4.7	5.4	0.6	1.1
Tl	1.4±0.7	0.5±0.5	0.8±0.5	1.4	0.8	1.4	1.2
Pb	187±96	116±132	91±54	425	127	2.6	1.0
Bi	7.3±5.4	9.1±13.0	3.0±2.2	36.9	6.5	7.2	2.3
Th	0.6±0.0	0.5±0.0	0.6±0.0	0.6	0.6	1.0	1.0
U	0.1±0.0	0.0±0.0	0.1±0.1	0.1	0.1	1.4	1.2

1137 Pre-SF indicated the period before 2014 Chinese Spring Festival (SF), covering the days from Jan. 24 to Jan. 29; SF indicated the Spring Festival period, covering
1138 the days from Jan. 30 to Feb.6; After-SF indicated the period after Spring Festival, covering the days from Feb.12 to Feb.21. CNY indicates the Chinese New Year
1139 (CNY) day and in 2014, it is Jan. 30; pre-CNY is the day before CNY and is Jan. 29. LF indicates the Lantern Festival (LF) day and in 2014, it is 14. Feb; pre-LF is
1140 the day before LF and is Feb.14. On CNY and LF, intensive fireworks were burned. Therefore, the mass concentrations of PM_{2.5} and associated chemical species of
1141 the two days were listed separately. CNY/pre-CNY indicates the ratios between mass concentrations of PM_{2.5} and associated chemical species on CNY and the day
1142 before CNY (pre-CNY). LF/pre-LF indicates the ratios between mass concentrations of PM_{2.5} and associated chemical species at LF and the day before LF
1143 (pre-LF).

1144

1145

1146

1147

1148 Table 2 Mass concentrations of ions and carbonaceous species in PM_{2.5} before, during and after 2014 Chinese Spring Festival at Nanjing ($\mu\text{g m}^{-3}$)

Elements	Pre-SF	SF (without CNY)	After-SF (without LF)	CNY	LF	CNY/pre-CNY	LF/pre-LF
Na ⁺	0.65±0.17	0.37±0.07	0.31±0.09	0.40	0.29	0.7	1.0
NH ₄ ⁺	4.26±1.12	4.81±3.68	5.33±1.98	10.5	6.85	2.4	1.3
K ⁺	0.49±0.31	1.59±1.55	0.67±0.22	4.81	1.06	8.9	1.8
Ca ²⁺	0.09±0.05	0.23±0.14	0.19±0.09	0.25	0.18	3.3	0.8
Mg ²⁺	0.03±0.03	0.20±0.31	0.08±0.04	0.10	0.09	1.3	1.5
F ⁻	0.03±0.01	0.04±0.02	0.03±0.01	0.05	0.04	2.2	1.4
Cl ⁻	1.16±0.26	0.72±0.54	0.75±0.40	3.04	1.09	3.8	1.2
NO ₂ ⁻	0.02±0.01	0.04±0.01	0.04±0.01	0.02	0.05	0.8	1.7
NO ₃ ⁻	5.81±2.54	5.27±5.38	6.59±2.98	14.6	8.36	2.5	1.3
SO ₄ ²⁻	3.46±1.28	7.74±5.17	4.05±2.34	16.1	4.54	4.4	1.1
OC	18.2±7.45	9.38±6.70	8.95±3.15	56.9	12.2	4.1	1.1
EC	6.93±4.64	3.12±3.06	2.96±1.20	8.29	3.38	1.8	0.9
OC1	1.87±1.40	0.40±0.23	0.50±0.16	16.1	0.64	33.2	1.1
OC2	4.32±1.65	2.56±1.75	2.36±0.74	14.8	2.86	4.2	1.1
OC3	5.46±2.69	2.77±2.09	2.90±1.15	9.10	4.28	2.4	1.0
OC4	5.44±1.52	3.27±3.03	2.94±1.36	5.81	4.46	0.9	1.1
EC1	7.92±5.07	3.44±2.64	3.15±1.00	18.8	3.30	4.1	0.9
EC2	0.12±0.07	0.07±0.06	0.06±0.05	0.50	0.08	37.7	1.6
EC3	0.00±0.00	0.00±0.00	0.00±0.00	0.11	0.00	-	-
OPC	1.12±2.43	0.39±0.39	0.24±0.43	11.09	0.00	-	-
PM _{2.5}	119.6±43.4	106.9±84.1	88.9±37.4	318.0	118.4	3.1	1.3

1149 - Not detected in the day before CNY and LF.

1150 Pre-SF indicated the period before 2014 Chinese Spring Festival (SF), covering the days from Jan. 24 to Jan. 29; SF indicated the Spring Festival period, covering

1151 the days from Jan. 30 to Feb.6; After-SF indicated the period after Spring Festival, covering the days from Feb.12 to Feb.21. CNY indicates the Chinese New Year

1152 (CNY) day and in 2014, it is Jan. 30; pre-CNY is the day before CNY and is Jan. 29. LF indicates the Lantern Festival (LF) day and in 2014, it is 14. Feb; pre-LF is
1153 the day before LF and is Feb.14. On CNY and LF, intensive fireworks were burned. Therefore, the mass concentrations of $PM_{2.5}$ and associated chemical species of
1154 the two days were listed seperately. CNY/pre-CNY indicates the ratios between mass concentrations of $PM_{2.5}$ and associated chemical species on CNY and the day
1155 before CNY (pre-CNY). LF/pre-LF indicates the ratios between mass concentrations of $PM_{2.5}$ and associated chemical species on LF and the day before LF
1156 (pre-LF).